IMA Journal of Numerical Analysis (2005) **25**, 113–138
doi: 10.1093/imanum/drh015

Semi-discrete central-upwind schemes with reduced dissipation for Hamilton–Jacobi equations

STEVE BRYSON†
Programme in Scientific Computing/Computational Mathematics, Stanford University and the NASA Advanced Supercomputing Division, NASA Ames Research Center, Moffett Field, CA 94035-1000, USA

ALEXANDER KURGANOV‡
Department of Mathematics, Tulane University, 6823 St. Charles Avenue, New Orleans, LA 70115, USA

DORON LEVY§
Department of Mathematics, Stanford University, Stanford, CA 94305-2125, USA

AND

GUERGANA PETROVA¶
Department of Mathematics, Texas A&M University, College Station, TX 77843-3368, USA

[Received on 18 February 2004; revised on 10 May 2004]

We introduce a new family of Godunov-type semi-discrete central schemes for multidimensional Hamilton–Jacobi equations. These schemes are a less dissipative generalization of the central-upwind schemes that have been recently proposed in Kurganov, Noelle and Petrova (2001, *SIAM J. Sci. Comput.*, **23**, pp. 707–740). We provide the details of the new family of methods in one, two, and three space dimensions, and then verify their expected low-dissipative property in a variety of examples.

Keywords: Hamilton–Jacobi equations; central-upwind schemes; semi-discrete methods.

1. Introduction

We consider the multidimensional Hamilton–Jacobi equation,

$$\varphi_t + H(\nabla_{\mathbf{x}}\varphi) = 0, \quad \mathbf{x} \in \mathbb{R}^d, \tag{1.1}$$

with Hamiltonian H. First-order numerical schemes that converge to the viscosity solution of (1.1) were first introduced by Crandall & Lions (1984) and by Souganidis (1985). Recent attempts to obtain higher-order approximate solutions of (1.1) include upwind methods (Jiang & Peng, 2000; Osher & Sethian, 1988; Osher & Shu, 1991), discontinuous Galerkin methods (Hu & Shu, 1999), and others. Here, we study a class of projection–evolution methods, called Godunov-type schemes. The main

†Email: bryson@nas.nasa.gov
‡Email: kurganov@math.tulane.edu
§Email: dlevy@math.stanford.edu
¶Email: gpetrova@math.tamu.edu

structure of these schemes is as follows: one starts with the point values of the solution, constructs an (essentially) non-oscillatory continuous piecewise polynomial interpolant, and then evolves it to the next time level while projecting the solution back onto the computational grid. The key idea in Godunov-type *central schemes* is to avoid solving (generalized) Riemann problems, by evolving (locally) smooth parts of the solution.

Second-order staggered Godunov-type central schemes were introduced by Lin & Tadmor (2001, 2000). L^1-convergence results for these schemes were obtained in Lin & Tadmor (2001). More efficient non-staggered central schemes as well as genuinely multidimensional generalizations of the schemes in Lin & Tadmor (2000) were presented in Bryson & Levy (2003a), with high-order extensions (up to fifth-order) proposed in Bryson & Levy (2003b,c).

Second-order semi-discrete Godunov-type central schemes were introduced in Kurganov & Tadmor (2000), where *local speeds* of propagation were employed to reduce the numerical dissipation. The numerical viscosity was further reduced in the *central-upwind* schemes (Kurganov *et al.*, 2001) by utilizing one-sided estimates of the local speeds of propagation. Higher-order extensions of these schemes were introduced in Bryson & Levy (2003d), where weighted essentially non-oscillatory (WENO) interpolants were used to increase accuracy. WENO interpolants were originally developed for numerical methods for hyperbolic conservation laws (Liu *et al.*, 1994; Jiang & Shu, 1996), and were first implemented in the context of upwind schemes for Hamilton–Jacobi equations in Jiang & Peng (2000).

Godunov-type central-upwind schemes are constructed in two steps. First, the solution is evolved to the next time level on a non-uniform grid (the location of the grid points depends on the local speeds, and thus can vary at every time step). The solution is then projected back onto the original grid. The projection step requires an additional piecewise polynomial reconstruction over the non-uniform grid. In this paper we show that in the semi-discrete setting different choices of such a reconstruction lead to different numerical Hamiltonians, and thus to different schemes. In particular, we can recover the scheme from Kurganov *et al.* (2001). A more careful selection of the reconstruction results in a new central-upwind scheme with smaller numerical dissipation. This approach was originally proposed in Kurganov & Petrova (2000), where it was applied to one-dimensional (1D) systems of hyperbolic conservation laws. It has been recently generalized and implemented for multidimensional systems of hyperbolic conservation laws in Kurganov & Lin (in preparation).

The paper is organized as follows. In Section 2, we develop new semi-discrete central-upwind schemes for 1D Hamilton–Jacobi equations. We also review the interpolants that are required to complete the construction of the second- and fifth-order schemes. Generalizations to more than one space dimension (with special emphasis on the two-dimensional setup) are then presented in Section 3, where the corresponding multidimensional interpolants are also discussed. In Section 4, we evaluate the performance of the new schemes with a series of numerical tests. Finally, in Appendix A, we prove the monotonicity of the new numerical Hamiltonian.

2. One-dimensional schemes

2.1 *Semi-discrete central-upwind schemes for Hamilton–Jacobi equations*

In this section, we describe the derivation of a new family of semi-discrete central-upwind schemes for the 1D Hamilton–Jacobi equation,

$$\varphi_t + H(\varphi_x) = 0, \qquad x \in \mathbb{R}, \tag{2.1}$$

subject to the initial data $\varphi(x, t=0) = \varphi_0(x)$. We follow the approach in Kurganov *et al.* (2001) (see also Kurganov & Tadmor, 2000). For simplicity we assume a uniform grid in space and time with grid spacing Δx and Δt, respectively. The grid points are denoted by $x_j := j\Delta x$, $t^n := n\Delta t$, and the approximate value of $\varphi\left(x_j, t^n\right)$ is denoted by φ_j^n.

Assume that the approximate solution at time t^n, φ_j^n, is given, and that a continuous piecewise-polynomial interpolant $\widetilde{\varphi}(x, t^n)$ is reconstructed from φ_j^n. At every grid point, the maximal right and left speeds of propagation, a_j^+ and a_j^-, are then estimated by

$$a_j^+ = \max_{\min\{\varphi_x^-,\varphi_x^+\}\leqslant u\leqslant\max\{\varphi_x^-,\varphi_x^+\}} \left\{H'(u), 0\right\}, \quad a_j^- = \left| \min_{\min\{\varphi_x^-,\varphi_x^+\}\leqslant u\leqslant\max\{\varphi_x^-,\varphi_x^+\}} \left\{H'(u), 0\right\} \right|, \tag{2.2}$$

where $\varphi_x^\pm$ are the one-sided derivatives at $x = x_j$, that is

$$\varphi_x^\pm := \widetilde{\varphi}_x(x_j \pm 0, t^n).$$

Obviously, the quantities $a_j^\pm$ also depend on time, and $\varphi_x^\pm$ depend on both time and location. These dependences are omitted to simplify the notation. If the Hamiltonian is convex, (2.2) reduces to

$$a_j^+ = \max\left\{H'(\varphi_x^-), H'(\varphi_x^+), 0\right\}, \quad a_j^- = \left|\min\left\{H'(\varphi_x^-), H'(\varphi_x^+), 0\right\}\right|, \tag{2.3}$$

while in the non-convex case, one has to use directly the expressions in (2.2).

We then proceed by evolving the reconstruction $\widetilde{\varphi}$ at the evolution points $x_{j\pm}^n := x_j \pm a_j^\pm \Delta t$, to the next time level according to (2.1). The time step Δt is chosen so that $x_{j+}^n < x_{(j+1)-}^n$ for all j. Therefore the solution remains smooth at $x_{j\pm}^n$ for $t \in [t^n, t^{n+1}]$ (see Fig. 1) and we can compute the values of the evolved solution $\{\varphi_{j\pm}^{n+1}\}$ by the Taylor expansion in time:

$$\varphi_{j\pm}^{n+1} = \widetilde{\varphi}(x_{j\pm}^n, t^n) - \Delta t H\left(\widetilde{\varphi}_x(x_{j\pm}^n, t^n)\right) + \mathcal{O}\left(\Delta t^2\right). \tag{2.4}$$

Using the values $\{\varphi_{j\pm}^{n+1}\}$ on the non-uniform grid $\{x_{j\pm}^n\}$, we construct a new quadratic interpolant $\widetilde{\psi}$. On the interval $[x_{j-}^n, x_{j+}^n]$, the interpolant takes the form

$$\widetilde{\psi}\left(x, t^{n+1}\right) := \varphi_{j-}^{n+1} + \frac{\varphi_{j+}^{n+1} - \varphi_{j-}^{n+1}}{x_{j+}^n - x_{j-}^n}\left(x - x_{j-}^n\right) + \frac{1}{2}(\widehat{\varphi}_{xx})_j^{n+1}(x - x_{j-}^n)(x - x_{j+}^n), \tag{2.5}$$

where $(\widehat{\varphi}_{xx})_j^{n+1}$ is yet to be determined and is an approximation to $\varphi_{xx}(\widehat{x}_j^n, t^{n+1})$, $\widehat{x}_j^n = (x_{j+}^n + x_{j-}^n)/2$. The projection back onto the original grid is then carried out by evaluating $\widetilde{\psi}(x, t^{n+1})$ at x_j,

$$\varphi_j^{n+1} := \widetilde{\psi}(x_j, t^{n+1}) = \frac{a_j^+}{a_j^+ + a_j^-}\varphi_{j-}^{n+1} + \frac{a_j^-}{a_j^+ + a_j^-}\varphi_{j+}^{n+1} - \frac{1}{2}(\widehat{\varphi}_{xx})_j^{n+1} a_j^+ a_j^- (\Delta t)^2. \tag{2.6}$$

Note that if the Riemann fan is symmetric, that is, if $a_j^+ = a_j^-$, then $\widehat{x}_j^n = x_j$. Substituting (2.4) in (2.6) yields

$$\begin{aligned}\varphi_j^{n+1} = {} & \frac{a_j^+}{a_j^+ + a_j^-}\left(\widetilde{\varphi}(x_{j-}^n, t^n) - \Delta t H(\widetilde{\varphi}_x(x_{j-}^n, t^n))\right) \\ & + \frac{a_j^-}{a_j^+ + a_j^-}\left(\widetilde{\varphi}(x_{j+}^n, t^n) - \Delta t H(\widetilde{\varphi}_x(x_{j+}^n, t^n))\right) - \frac{1}{2}(\widehat{\varphi}_{xx})_j^{n+1} a_j^+ a_j^- (\Delta t)^2 + \mathcal{O}(\Delta t)^2. \end{aligned} \tag{2.7}$$

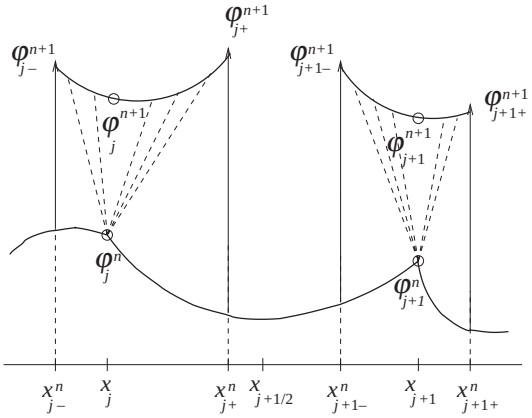

FIG. 1. Central-upwind differencing: 1D.

Using the Taylor expansion in space,

$$\widetilde{\varphi}(x^n_{j\pm}, t^n) = \varphi^n_j \pm \Delta t a^{\pm}_j \varphi^{\pm}_x + \mathcal{O}(\Delta t)^2, \tag{2.8}$$

we arrive at

$$\varphi^{n+1}_j = \varphi^n_j + \Delta t \frac{a^+_j a^-_j}{a^+_j + a^-_j}\left(\varphi^+_x - \varphi^-_x\right) - \frac{\Delta t}{a^+_j + a^-_j}\Big[a^-_j H(\widetilde{\varphi}_x(x^n_{j+}, t^n)) + a^+_j H(\widetilde{\varphi}_x(x^n_{j-}, t^n))\Big]$$
$$-\frac{1}{2}(\widehat{\varphi}_{xx})^{n+1}_j a^+_j a^-_j (\Delta t)^2 + \mathcal{O}(\Delta t)^2. \tag{2.9}$$

We then let $\Delta t \to 0$, and end up with the (family of) semi-discrete central-upwind schemes:

$$\frac{\mathrm{d}}{\mathrm{d}t}\varphi_j(t) = -\frac{a^-_j H(\varphi^+_x) + a^+_j H(\varphi^-_x)}{a^+_j + a^-_j} + a^+_j a^-_j \left(\frac{\varphi^+_x - \varphi^-_x}{a^+_j + a^-_j} - \frac{1}{2}\lim_{\Delta t\to 0}\Big[\Delta t(\widehat{\varphi}_{xx})^{n+1}_j\Big]\right). \tag{2.10}$$

Here, the one-sided speeds of propagation, $a^{\pm}_j$, are given by (2.2), and $\varphi^{\pm}_x$ are the left and right derivatives at the point $x = x_j$ of the reconstruction $\widetilde{\varphi}(\cdot, t)$ at time t.

Finally, in order to complete the construction of the scheme, we must determine $(\widehat{\varphi}_{xx})^{n+1}_j$. For example, selecting $(\widehat{\varphi}_{xx})^{n+1}_j$ to be independent of Δt gives

$$\lim_{\Delta t\to 0}\Big[\Delta t(\widehat{\varphi}_{xx})^{n+1}_j\Big] = 0,$$

and then (2.10) recovers the central-upwind scheme in Kurganov *et al.* (2001). However, since the interpolant $\widetilde{\psi}(\cdot, t^{n+1})$ is defined on the intervals $[x^n_{j-}, x^n_{j+}]$, whose size is proportional to Δt, it is natural to choose $(\widehat{\varphi}_{xx})^{n+1}_j$ to be proportional to $1/\Delta t$. In this case, the approximation of the second derivative in (2.10) will add a non-zero contribution to the limit as $\Delta t \to 0$. At the same time, to guarantee a

non-oscillatory reconstruction, we should use a nonlinear limiter. For example, one can use the minmod limiter:

$$\Delta t(\widehat{\varphi}_{xx})_j^{n+1} = 2\,\text{minmod}\left(\frac{\widetilde{\varphi}_x(x_{j+}^n, t^{n+1}) - \widetilde{\psi}_x(\widehat{x}_j^n, t^{n+1})}{a_j^+ + a_j^-}, \frac{\widetilde{\psi}_x(\widehat{x}_j^n, t^{n+1}) - \widetilde{\varphi}_x(x_{j-}^n, t^{n+1})}{a_j^+ + a_j^-}\right), \quad (2.11)$$

where $\widetilde{\psi}_x$ is the derivative of (2.5), $\widetilde{\varphi}_x(x_{j\pm}^n, t^{n+1})$ are the values of the derivative of the evolved reconstruction $\widetilde{\varphi}(\cdot, t^n)$ at $t = t^{n+1}$, and the multivariate minmod function is defined by

$$\text{minmod}(x_1, x_2, \dots) := \begin{cases} \min\limits_j\{x_j\}, & \text{if } x_j > 0 \ \forall j, \\ \max\limits_j\{x_j\}, & \text{if } x_j < 0 \ \forall j, \\ 0, & \text{otherwise.} \end{cases} \quad (2.12)$$

A different choice of limiter in (2.11) will result in a different scheme from the same family of central-upwind schemes.

All that remains is to determine the quantities used in (2.11). Since all data are smooth along the line segments $(x_{j\pm}^n, t)$, $t^n \leqslant t < t^{n+1}$, we can use a Taylor expansion in time to obtain

$$\widetilde{\varphi}_x(x_{j\pm}^n, t^{n+1}) = \widetilde{\varphi}_x(x_{j\pm}^n, t^n) + \mathcal{O}(\Delta t). \quad (2.13)$$

According to (2.5), the derivative $\widetilde{\psi}_x(\widehat{x}_j^n, t^{n+1})$ of the new reconstruction $\widetilde{\psi}$ at time level t^{n+1} is

$$\widetilde{\psi}_x(\widehat{x}_j^n, t^{n+1}) = \frac{\varphi_{j+}^{n+1} - \varphi_{j-}^{n+1}}{(a_j^+ + a_j^-)\Delta t}, \quad (2.14)$$

and after substituting (2.4) and (2.8) into (2.14), we obtain

$$\widetilde{\psi}_x(\widehat{x}_j^n, t^{n+1}) = \frac{a_j^+\varphi_x^+ + a_j^-\varphi_x^-}{(a_j^+ + a_j^-)} - \frac{H(\widetilde{\varphi}_x(x_{j+}^n, t^n)) - H(\widetilde{\varphi}_x(x_{j-}^n, t^n))}{(a_j^+ + a_j^-)} + \mathcal{O}(\Delta t). \quad (2.15)$$

Passing to the semi-discrete limit ($\Delta t \to 0$) in (2.11), (2.13), and (2.15) gives

$$\lim_{\Delta t\to 0}\left[\Delta t(\widehat{\varphi}_{xx})_j^{n+1}\right] = \frac{2}{(a_j^+ + a_j^-)}\,\text{minmod}\left(\varphi_x^+ - \psi_x^{\text{int}}, \psi_x^{\text{int}} - \varphi_x^-\right), \quad (2.16)$$

where

$$\psi_x^{\text{int}} := \lim_{\Delta t\to 0}[\widetilde{\psi}_x(\widehat{x}_j^n, t^{n+1})] = \frac{a_j^+\varphi_x^+ + a_j^-\varphi_x^-}{(a_j^+ + a_j^-)} - \frac{H(\varphi_x^+) - H(\varphi_x^-)}{(a_j^+ + a_j^-)}. \quad (2.17)$$

Finally, substituting (2.16) into (2.10), we obtain the 1D *low-dissipative semi-discrete central-upwind scheme*:

$$\frac{\mathrm{d}}{\mathrm{d}t}\varphi_j(t) = -\frac{a_j^- H(\varphi_x^+) + a_j^+ H(\varphi_x^-)}{a_j^+ + a_j^-} + a_j^+ a_j^-\left[\frac{\varphi_x^+ - \varphi_x^-}{a_j^+ + a_j^-} - \text{minmod}\left(\frac{\varphi_x^+ - \psi_x^{\text{int}}}{a_j^+ + a_j^-}, \frac{\psi_x^{\text{int}} - \varphi_x^-}{a_j^+ + a_j^-}\right)\right], \quad (2.18)$$

where ψ_x^{int} is given by (2.17). For future reference, we denote the RHS of (2.18) by $-H^{BKLP}$.

Notice that in the fully-discrete setting the use of the intermediate quadratic reconstruction $\widetilde{\psi}(\cdot, t^{n+1})$ at level t^{n+1} (as opposed to the intermediate piecewise linear reconstruction in Kurganov *et al.*, 2001) increases the accuracy of the resulting fully-discrete scheme: $\mathcal{O}((\Delta t)^2 + (\Delta x)^r)$ versus $\mathcal{O}(\Delta t + (\Delta x)^r)$, where r is the (formal) order of accuracy of the continuous piecewise polynomial reconstruction $\widetilde{\varphi}(\cdot, t^n)$. When we pass to the semi-discrete limit ($\Delta t \to 0$), both quadratic and linear interpolation errors go to 0, and therefore the (formal) order of accuracy of both (2.17)–(2.18) and the semi-discrete scheme in Kurganov *et al.* (2001) is $\mathcal{O}((\Delta x)^r)$. The temporal error is determined solely by the (formal) order of accuracy of the ODE solver used to integrate (2.18). However, the minmod limiter introduces a new term that leads to a reduction of the numerical dissipation without affecting the accuracy of the scheme. To demonstrate this, we show that ψ_x^{int} is always in the interval $[\min\{\varphi_x^+, \varphi_x^-\}, \max\{\varphi_x^+, \varphi_x^-\}]$, and therefore the absolute value of the term $(\varphi_x^+ - \varphi_x^-)$ in the numerical dissipation in the scheme from Kurganov *et al.* (2001) is always greater than the absolute value of the new term, that is

$$\left|\varphi_x^+ - \varphi_x^-\right| \geqslant \left|\varphi_x^+ - \varphi_x^- - \text{minmod}\left(\varphi_x^+ - \psi_x^{\text{int}}, \psi_x^{\text{int}} - \varphi_x^-\right)\right|.$$

Indeed, we have

$$\psi_x^{\text{int}} = \frac{a_j^+ \varphi_x^+ + a_j^- \varphi_x^-}{(a_j^+ + a_j^-)} - \frac{H(\varphi_x^+) - H(\varphi_x^-)}{(a_j^+ + a_j^-)} = \varphi_x^+ \left[\frac{a_j^+ - H'(\xi)}{a_j^+ + a_j^-}\right] + \varphi_x^- \left[\frac{H'(\xi) + a_j^-}{a_j^+ + a_j^-}\right], \quad (2.19)$$

where $\xi \in (\min\{\varphi_x^+, \varphi_x^-\}, \max\{\varphi_x^+, \varphi_x^-\})$. It follows from the definition of the local speeds (2.2) that

$$a_j^+ - H'(\xi) \geqslant 0, \quad H'(\xi) + a_j^- \geqslant 0.$$

Thus, (2.19) is a convex combination of φ_x^+ and φ_x^-, and therefore $\psi_x^{\text{int}} \in [\min\{\varphi_x^+, \varphi_x^-\}, \max\{\varphi_x^+, \varphi_x^-\}]$.

Remarks.

1. We would like to emphasize that the reduced dissipation in the scheme (2.18) when compared with the scheme of Kurganov *et al.* (2001) is due to the minmod term in the RHS of (2.18). This additional term arises when we define $(\hat{\varphi}_{xx})_j^{n+1}$ by (2.11) such that the $\lim_{\Delta t \to 0}\left[\Delta t (\widehat{\varphi}_{xx})_j^{n+1}\right]$ in (2.10) does not vanish.
2. While the new nonlinear limiters in the scheme (2.18) require additional computational work, the quantities that participate in the limiter do not require any new flux evaluations and hence the increase in the computational complexity is minimal. Such additional work (when compared with the original scheme of Kurganov *et al.*, 2001) can be worthwhile in cases where the user is interested in increasing the resolution of the solution without increasing the order of accuracy of the method.

It was shown in Bryson & Levy (2003d) that the numerical Hamiltonian H^{KNP} from Kurganov *et al.* (2001) is monotone, provided that the Hamiltonian H is convex. Here, we state a theorem about the monotonicity of H^{BKLP}—the new, less dissipative Hamiltonian in (2.18). The proof is left to the Appendix. We will consider only Hamiltonians for which H' changes sign, because otherwise either $a^- \equiv 0$ or $a^+ \equiv 0$ and the Hamiltonian in (2.18) reduces to the upwind one for which such a theorem is known.

THEOREM 2.1 Let the Hamiltonian $H \in C^2$ be convex and satisfy the following two assumptions:

(A1) The function

$$G(u,v) := 2H''(u)\big[(u-v)H'(v) - (H(u)-H(v))\big] + \big[H'(u)-H'(v)\big]^2 \leqslant 0 \tag{2.20}$$

for all u and v in the set $S^-(u,v) \cup S^+(u,v)$, where

$$\begin{aligned} S^-(u,v) &:= \left\{(u,v) : \frac{H(u)-H(v)}{u-v} \leqslant \frac{H'(u)+H'(v)}{2},\ u \geqslant u^* \geqslant v\right\},\\ S^+(u,v) &:= \left\{(u,v) : \frac{H(u)-H(v)}{u-v} \geqslant \frac{H'(u)+H'(v)}{2},\ u \leqslant u^* \leqslant v\right\}, \end{aligned} \tag{2.21}$$

and u^* is the only point such that $H'(u^*) = 0$;

(A2) For any v and for an arbitrary interval $[a,b]$, the sets $S^-(u,v) \cap [a,b]$ and $S^+(u,v) \cap [a,b]$ are either the empty set or finite unions of closed intervals and/or points.

Then the numerical Hamiltonian in (2.18):

$$\begin{aligned} H^{BKLP}(u^+,u^-) := &\frac{a^-H(u^+) + a^+H(u^-)}{a^+ + a^-}\\ &- a^+a^-\left[\frac{u^+-u^-}{a^+ + a^-} - \operatorname{minmod}\left(\frac{u^+-u^{\text{int}}}{a^+ + a^-}, \frac{u^{\text{int}}-u^-}{a^+ + a^-}\right)\right], \end{aligned} \tag{2.22}$$

where

$$u^{\text{int}} := \frac{a^+u^+ + a^-u^-}{(a^+ + a^-)} - \frac{H(u^+) - H(u^-)}{(a^+ + a^-)},$$

and where $a^+ := a^+(u^+,u^-) = \max\{H'(u^+), H'(u^-), 0\}$, $a^- := a^-(u^+,u^-) = |\min\{H'(u^+), H'(u^-), 0\}|$ is monotone, that is H^{BKLP} is a non-increasing function of u^+ and a non-decreasing function of u^-.

Remarks.

1. Examples of Hamiltonian that satisfy conditions (2.20)–(2.21) are any convex quadratic Hamiltonian $H(u) = au^2 + bu + c$. Straightforward computation gives that the function $G(u,v) \equiv 0$, and the sets in (A2) are either empty or one closed interval, or one point, and therefore the theorem holds. Another example, for which Theorem 2.1 is valid, is $H(u) = u^4$. In this case, the sets (2.21) are

$$S^-(u,v) = \{(u,v) : u+v \geqslant 0 \geqslant v\}, \quad S^+(u,v) = \{(u,v) : u+v \leqslant 0 \leqslant v\},$$

and, as one can easily verify, the function

$$G(u,v) = -8(u-v)^3(u^3 + 3u^2v + 6uv^2 + 2v^3) \leqslant 0,$$

in $S^-(u,v) \cup S^+(u,v)$. As for the sets in assumption (A2), they are either empty or one closed interval, or one point.

2. Notice that assumption (A2) in Theorem 2.1 is needed only for technical purposes and in fact it is satisfied by (almost) every Hamiltonian H that arises in applications.

3. The monotonicity of the numerical Hamiltonian is an essential ingredient in the theory of Barles & Souganidis (1991). The main theorem in Barles & Souganidis (1991) implies that a consistent, stable and monotone approximation of a Hamilton–Jacobi equation that satisfies an underlying comparison principle converges to the unique viscosity solution of that equation. In our context, such an approximation can be obtained if we assume a piecewise-linear reconstruction and replace the time derivative by a forward Euler approximation.

2.2 *A second-order scheme*

A non-oscillatory second-order scheme can be obtained if one uses a non-oscillatory continuous piecewise quadratic interpolant $\widetilde{\varphi}$. The values of the one-sided derivatives of $\widetilde{\varphi}$ at (x_j, t^n) in (2.17) and (2.18) are given by

$$\varphi_x^{\pm} = \frac{(\Delta\varphi)^n_{j\pm\frac{1}{2}}}{\Delta x} \mp \frac{\Delta x}{2}\,(\varphi_{xx})^n_{j+\frac{1}{2}}\,, \qquad (\Delta\varphi)^n_{j+\frac{1}{2}} := \varphi^n_{j+1} - \varphi^n_j, \tag{2.23}$$

where the second derivative is computed with a nonlinear limiter. For example,

$$(\varphi_{xx})^n_{j+\frac{1}{2}} = \text{minmod}\left(\theta\frac{(\Delta\varphi)^n_{j+\frac{3}{2}} - (\Delta\varphi)^n_{j+\frac{1}{2}}}{(\Delta x)^2}, \frac{(\Delta\varphi)^n_{j+\frac{3}{2}} - (\Delta\varphi)^n_{j-\frac{1}{2}}}{2(\Delta x)^2}, \theta\frac{(\Delta\varphi)^n_{j+\frac{1}{2}} - (\Delta\varphi)^n_{j-\frac{1}{2}}}{(\Delta x)^2}\right). \tag{2.24}$$

Here, $\theta \in [1, 2]$ and the minmod function is given by (2.12). As is well-known, larger values of θ correspond to less dissipative limiters (see Sweby, 1984). The scheme requires an ODE solver that is at least second-order accurate.

2.3 *Higher-order schemes*

In this section, we briefly describe the third- and fifth-order WENO reconstructions. They were derived in Bryson & Levy (2003d) in the context of central-upwind schemes, and are similar to those used in high-order upwind schemes (Jiang & Peng, 2000).

In smooth regions, the WENO reconstructions use a convex combination of multiple overlapping reconstructions to attain high-order accuracy. In non-smooth regions, a smoothness measure is employed to increase the weight of the least oscillatory reconstruction. Here, we reconstruct the one-sided derivatives $(\varphi_x^{\pm})_{k,j}$ at $x = x_j$ for $k = 1, \ldots, d$ stencils, and write the convex combination

$$\varphi_x^{\pm} = \sum_{k=1}^{d} w^{\pm}_{k,j}(\varphi_x^{\pm})_{k,j}, \qquad \sum_{k=1}^{d} w^{\pm}_{k,j} = 1, \qquad w^{\pm}_{k,j} \geqslant 0, \tag{2.25}$$

where the values $\varphi_x^{\pm}$ are to be used in the scheme (2.17)–(2.18). The weights $w^{\pm}_{k,j}$ are defined as

$$w^{\pm}_{k,j} = \frac{\alpha^{\pm}_{k,j}}{\sum_{l=1}^{d}\alpha^{\pm}_{l,j}}, \qquad \alpha^{\pm}_{k,j} = \frac{c^{\pm}_k}{\left(\epsilon + S^{\pm}_{k,j}\right)^p}. \tag{2.26}$$

The constants $c_k^{\pm}$ are set so that the convex combination in (2.25) is of the maximal possible order of accuracy in smooth regions. We take $p = 2$ and choose $\epsilon = 10^{-6}$ to prevent the denominator in (2.26) from vanishing.

A third-order WENO reconstruction is obtained in the case $d = 2$ with

$$(\varphi_x^+)_{1,j} = \frac{\varphi_{j+1} - \varphi_{j-1}}{2\Delta x}, \qquad (\varphi_x^-)_{1,j} = \frac{-\varphi_{j-2} + 4\varphi_{j-1} - 3\varphi_j}{2\Delta x},$$
$$(\varphi_x^+)_{2,j} = \frac{-3\varphi_j + 4\varphi_{j+1} - \varphi_{j+2}}{2\Delta x}, \qquad (\varphi_x^-)_{2,j} = \frac{\varphi_{j+1} - \varphi_{j-1}}{2\Delta x}.$$

The constants $c_k^{\pm}$ are given by

$$c_1^+ = c_2^- = \frac{2}{3}, \quad c_2^+ = c_1^- = \frac{1}{3},$$

and the smoothness measures are

$$S_{1,j}^+ = S_j[-1, 0], \quad S_{2,j}^+ = S_j[0, 1], \quad S_{1,j}^- = S_j[-2, -1], \quad S_{2,j}^- = S_j[-1, 0].$$

Here,

$$S_j[r, s] := \Delta x \sum_{i=r}^{s} \left(\frac{\Delta^+ \varphi_{j+i}}{\Delta x}\right)^2 + \Delta x \sum_{i=r+1}^{s} \left(\frac{\Delta^+ \Delta^- \varphi_{j+i}}{\Delta x^2}\right)^2, \quad \Delta^{\pm}\varphi_j := \pm(\varphi_{j\pm1} - \varphi_j). \tag{2.27}$$

A fifth-order WENO reconstruction is obtained when $d = 3$. In this case,

$$(\varphi_x^+)_{1,j} = \frac{\varphi_{j-2} - 6\varphi_{j-1} + 3\varphi_j + 2\varphi_{j+1}}{6\Delta x}, \qquad (\varphi_x^-)_{1,j} = \frac{2\varphi_{j-3} - 9\varphi_{j-2} + 18\varphi_{j-1} - 11\varphi_j}{6\Delta x},$$
$$(\varphi_x^+)_{2,j} = \frac{-2\varphi_{j-1} - 3\varphi_j + 6\varphi_{j+1} - \varphi_{j+2}}{6\Delta x}, \qquad (\varphi_x^-)_{2,j} = \frac{-\varphi_{j-2} + 6\varphi_{j-1} - 3\varphi_j - 2\varphi_{j+1}}{6\Delta x},$$
$$(\varphi_x^+)_{3,j} = \frac{-11\varphi_j + 18\varphi_{j+1} - 9\varphi_{j+2} + 2\varphi_{j+3}}{6\Delta x}, \qquad (\varphi_x^-)_{3,j} = \frac{2\varphi_{j-1} + 3\varphi_j - 6\varphi_{j+1} + \varphi_{j+2}}{6\Delta x}.$$

The constants $c_k^{\pm}$ are given by

$$c_1^+ = c_3^- = \frac{3}{10}, \quad c_3^+ = c_1^- = \frac{1}{10}, \quad c_2^{\pm} = \frac{3}{5},$$

and the smoothness measures are

$$S_{1,j}^+ = S_j[-2, 0], \quad S_{2,j}^+ = S_j[-1, 1], \quad S_{3,j}^+ = S_j[0, 2],$$
$$S_{1,j}^- = S_j[-3, -1], \quad S_{2,j}^- = S_j[-2, 0], \quad S_{3,j}^- = S_j[-1, 1].$$

The time evolution of (2.18) should be performed with an ODE solver whose order of accuracy is compatible with the spatial order of the scheme. In our numerical examples, we use the strong stability preserving (SSP) Runge–Kutta methods from Gottlieb *et al.* (2001).

3. Multidimensional schemes

In this section, we derive the two-dimensional (2D) generalization of the semi-discrete central-upwind scheme (2.17)–(2.18) and then extend it to three space dimensions. We also comment on the multidimensional interpolants that these extensions require.

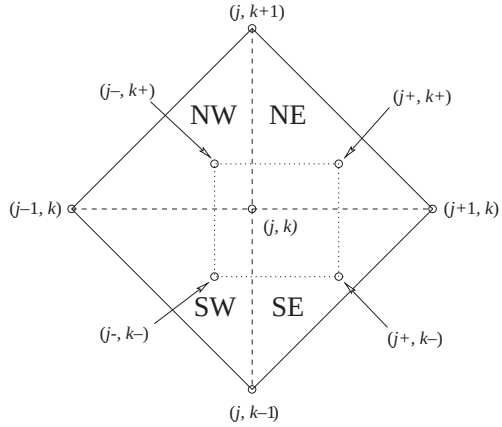

FIG. 2. Central-upwind differencing: 2D.

3.1 *A two-dimensional scheme*

We consider the 2D Hamilton–Jacobi equation,

$$\varphi_t + H(\varphi_x, \varphi_y) = 0, \tag{3.1}$$

and proceed as in Kurganov *et al.* (2001). We assume that at time $t = t^n$ the approximate point values $\varphi^n_{jk} \approx \varphi(x_j, y_k, t^n)$ are given, and construct a 2D continuous piecewise-quadratic interpolant, $\widetilde{\varphi}(x, y, t^n)$, defined on the cells $S_{jk} := \{(x, y) : \frac{|x-x_j|}{\Delta x} + \frac{|y-y_k|}{\Delta y} \leqslant 1\}$. On each cell S_{jk} there will be four such interpolants (labelled NW, NE, SE, and SW), one for each triangle that constitutes S_{jk} (see Fig. 2). Specific examples of $\widetilde{\varphi}(x, y, t^n)$ are discussed in Section 3.3.

Similarly to the 1D case, we use the maximal values of the one-sided local speeds of propagation in the x- and y-directions to estimate the widths of the local Riemann fans. These values at any grid point (x_j, y_k) can be computed as

$$\begin{aligned} a^+_{jk} &:= \max_{C_{jk}} \left\{ H_u(\widetilde{\varphi}_x(x, y, t), \widetilde{\varphi}_y(x, y, t)) \right\}_+, \quad a^-_{jk} := \left| \min_{C_{jk}} \left\{ H_u(\widetilde{\varphi}_x(x, y, t), \widetilde{\varphi}_y(x, y, t)) \right\}_- \right|, \\ b^+_{jk} &:= \max_{C_{jk}} \left\{ H_v(\widetilde{\varphi}_x(x, y, t), \widetilde{\varphi}_y(x, y, t)) \right\}_+, \quad b^-_{jk} := \left| \min_{C_{jk}} \left\{ H_v(\widetilde{\varphi}_x(x, y, t), \widetilde{\varphi}_y(x, y, t)) \right\}_- \right|, \end{aligned} \tag{3.2}$$

where $C_{jk} := [x_{j-\frac{1}{2}}, x_{j+\frac{1}{2}}] \times [y_{k-\frac{1}{2}}, y_{k+\frac{1}{2}}]$, $(\cdot)_+ := \max(\cdot, 0)$, $(\cdot)_- := \min(\cdot, 0)$, and $(H_u, H_v)^T$ is the gradient of H. Note that in order to obtain a monotone scheme in two dimensions, one may need to use global a priori bounds on some of the derivatives in (3.2) (see Osher & Shu, 1991 for details).

The reconstruction $\widetilde{\varphi}(x, y, t^n)$ is then evolved according to the Hamilton–Jacobi equation (3.1). Due to the finite speed of propagation, for sufficiently small Δt, the solution of (3.1) with initial data $\widetilde{\varphi}$ is smooth around $(x^n_{j\pm}, y^n_{k\pm})$ where $x^n_{j\pm} := x_j \pm a^\pm_{jk}\Delta t$, $y^n_{k\pm} := y_k \pm b^\pm_{jk}\Delta t$, see Fig. 2. We denote $\widetilde{\varphi}^n_{j\pm,k\pm} := \widetilde{\varphi}(x^n_{j\pm}, y^n_{k\pm}, t^n)$, and use the Taylor expansion to calculate the intermediate values at the next

time level $t = t^{n+1}$:

$$\varphi^{n+1}_{j\pm,k\pm} = \widetilde{\varphi}^{n}_{j\pm,k\pm} - \Delta t \cdot H(\widetilde{\varphi}_x(x^n_{j\pm}, y^n_{k\pm}, t^n), \widetilde{\varphi}_y(x^n_{j\pm}, y^n_{k\pm}, t^n)) + \mathcal{O}(\Delta t)^2. \tag{3.3}$$

We now project the intermediate values $\varphi^{n+1}_{j\pm,k\pm}$ onto the original grid points (x_j, y_k). First, similarly to (2.5), we use new 1D quadratic interpolants in the y-direction, $\widetilde{\psi}(x^n_{j\pm}, \cdot, t^{n+1})$, to obtain

$$\begin{aligned}\widetilde{\psi}(x^n_{j\pm}, y_k, t^{n+1}) &= \varphi^{n+1}_{j\pm,k-} + \frac{\varphi^{n+1}_{j\pm,k+} - \varphi^{n+1}_{j\pm,k-}}{b^+_{jk} + b^-_{jk}} b^-_{jk} - \frac{1}{2}(\widehat{\varphi}_{yy})^{n+1}_{j\pm,k} b^+_{jk} b^-_{jk} (\Delta t)^2 \\ &= \frac{b^+_{jk}}{b^+_{jk} + b^-_{jk}} \varphi^{n+1}_{j\pm,k-} + \frac{b^-_{jk}}{b^+_{jk} + b^-_{jk}} \varphi^{n+1}_{j\pm,k+} - \frac{1}{2}(\widehat{\varphi}_{yy})^{n+1}_{j\pm,k} b^+_{jk} b^-_{jk} (\Delta t)^2, \end{aligned} \tag{3.4}$$

where $(\widehat{\varphi}_{yy})^{n+1}_{j\pm,k} \approx \varphi_{yy}(x^n_{j\pm}, \widehat{y}^n_k, t^{n+1})$ and $\widehat{y}^n_k := (y^n_{k+} + y^n_{k-})/2$. Next, we use the values $\widetilde{\psi}(x^n_{j\pm}, y_k, t^{n+1})$ to construct another 1D quadratic interpolant $\widetilde{\psi}(\cdot, y_k, t^{n+1})$, this time in the x-direction, whose values at the original grid points are

$$\begin{aligned}\varphi^{n+1}_{jk} &:= \widetilde{\psi}(x_j, y_k, t^{n+1}) \\ &= \frac{a^+_{jk}}{a^+_{jk} + a^-_{jk}} \widetilde{\psi}(x^n_{j-}, y_k, t^{n+1}) + \frac{a^-_{jk}}{a^+_{jk} + a^-_{jk}} \widetilde{\psi}(x^n_{j+}, y_k, t^{n+1}) - \frac{1}{2}(\widehat{\varphi}_{xx})^{n+1}_{j,k} a^+_{jk} a^-_{jk} (\Delta t)^2. \end{aligned} \tag{3.5}$$

Here, $(\widehat{\varphi}_{xx})^{n+1}_{j,k} \approx \varphi_{xx}(\widehat{x}^n_j, y_k, t^{n+1})$ and $\widehat{x}^n_j := (x^n_{j+} + x^n_{j-})/2$. We choose $(\widehat{\varphi}_{xx})^{n+1}_{j,k}$ to be the weighted average

$$(\widehat{\varphi}_{xx})^{n+1}_{j,k} = \frac{b^+_{jk}}{b^+_{jk} + b^-_{jk}} (\widehat{\varphi}_{xx})^{n+1}_{j,k-} + \frac{b^-_{jk}}{b^+_{jk} + b^-_{jk}} (\widehat{\varphi}_{xx})^{n+1}_{j,k+}, \qquad (\widehat{\varphi}_{xx})^{n+1}_{j,k\pm} \approx \varphi_{xx}(\widehat{x}^n_j, y^n_{k\pm}, t^{n+1}). \tag{3.6}$$

Notice that both $(\widehat{\varphi}_{yy})^{n+1}_{j\pm,k}$ in (3.4) and $(\widehat{\varphi}_{xx})^{n+1}_{j,k\pm}$ in (3.6) are yet to be determined.

We then substitute (3.4) and (3.6) into (3.5), and obtain

$$\begin{aligned}\varphi^{n+1}_{jk} = {} & \frac{a^-_{jk} b^-_{jk} \varphi^{n+1}_{j+,k+} + a^-_{jk} b^+_{jk} \varphi^{n+1}_{j+,k-} + a^+_{jk} b^-_{jk} \varphi^{n+1}_{j-,k+} + a^+_{jk} b^+_{jk} \varphi^{n+1}_{j-,k-}}{(a^+_{jk} + a^-_{jk})(b^+_{jk} + b^-_{jk})} \\ & - \frac{a^+_{jk} a^-_{jk}}{b^+_{jk} + b^-_{jk}} \left[b^+_{jk} (\widehat{\varphi}_{xx})^{n+1}_{j,k-} + b^-_{jk} (\widehat{\varphi}_{xx})^{n+1}_{j,k+} \right] \frac{(\Delta t)^2}{2} \\ & - \frac{b^+_{jk} b^-_{jk}}{a^+_{jk} + a^-_{jk}} \left[a^+_{jk} (\widehat{\varphi}_{yy})^{n+1}_{j-,k} + a^-_{jk} (\widehat{\varphi}_{yy})^{n+1}_{j+,k} \right] \frac{(\Delta t)^2}{2} + \mathcal{O}(\Delta t)^2. \end{aligned} \tag{3.7}$$

Substituting (3.3) into (3.7) yields

$$\begin{aligned}
\varphi_{jk}^{n+1} = {} & \frac{a_{jk}^- b_{jk}^-}{(a_{jk}^+ + a_{jk}^-)(b_{jk}^+ + b_{jk}^-)} \Big(\widetilde{\varphi}_{j+,k+}^n - \Delta t \cdot H(\widetilde{\varphi}_x(x_{j+}^n, y_{k+}^n, t^n), \widetilde{\varphi}_y(x_{j+}^n, y_{k+}^n, t^n)) \Big) \\
& + \frac{a_{jk}^- b_{jk}^+}{(a_{jk}^+ + a_{jk}^-)(b_{jk}^+ + b_{jk}^-)} \Big(\widetilde{\varphi}_{j+,k-}^n - \Delta t \cdot H(\widetilde{\varphi}_x(x_{j+}^n, y_{k-}^n, t^n), \widetilde{\varphi}_y(x_{j+}^n, y_{k-}^n, t^n)) \Big) \\
& + \frac{a_{jk}^+ b_{jk}^-}{(a_{jk}^+ + a_{jk}^-)(b_{jk}^+ + b_{jk}^-)} \Big(\widetilde{\varphi}_{j-,k+}^n - \Delta t \cdot H(\widetilde{\varphi}_x(x_{j-}^n, y_{k+}^n, t^n), \widetilde{\varphi}_y(x_{j-}^n, y_{k+}^n, t^n)) \Big) \\
& + \frac{a_{jk}^+ b_{jk}^+}{(a_{jk}^+ + a_{jk}^-)(b_{jk}^+ + b_{jk}^-)} \Big(\widetilde{\varphi}_{j-,k-}^n - \Delta t \cdot H(\widetilde{\varphi}_x(x_{j-}^n, y_{k-}^n, t^n), \widetilde{\varphi}_y(x_{j-}^n, y_{k-}^n, t^n)) \Big) \\
& - \frac{a_{jk}^+ a_{jk}^-}{b_{jk}^+ + b_{jk}^-} \left[b_{jk}^+ (\widehat{\varphi}_{xx})_{j,k-}^{n+1} + b_{jk}^- (\widehat{\varphi}_{xx})_{j,k+}^{n+1} \right] \frac{(\Delta t)^2}{2} \\
& - \frac{b_{jk}^+ b_{jk}^-}{a_{jk}^+ + a_{jk}^-} \left[a_{jk}^+ (\widehat{\varphi}_{yy})_{j-,k}^{n+1} + a_{jk}^- (\widehat{\varphi}_{yy})_{j+,k}^{n+1} \right] \frac{(\Delta t)^2}{2} + \mathcal{O}(\Delta t)^2. \qquad (3.8)
\end{aligned}$$

The values $\widetilde{\varphi}_{j\pm,k\pm}^n$ are computed by the Taylor expansions:

$$\widetilde{\varphi}_{j\pm,k\pm}^n = \varphi_{j,k}^n \pm \Delta t a_{jk}^{\pm} \varphi_x^{\pm} \pm \Delta t b_{jk}^{\pm} \varphi_y^{\pm} + \mathcal{O}(\Delta t)^2, \qquad (3.9)$$

where $\varphi_x^{\pm} := \widetilde{\varphi}_x(x_j \pm 0, y_k, t^n)$ and $\varphi_y^{\pm} := \widetilde{\varphi}_y(x_j, y_k \pm 0, t^n)$ are the corresponding right and left derivatives of the continuous piecewise quadratic reconstruction at (x_j, y_k).

Next, substituting (3.9) into (3.8) gives

$$\begin{aligned}
\varphi_{jk}^{n+1} = {} & \varphi_{jk}^n + \Delta t \frac{a_{jk}^+ a_{jk}^-}{a_{jk}^+ + a_{jk}^-} (\varphi_x^+ - \varphi_x^-) + \Delta t \frac{b_{jk}^+ b_{jk}^-}{b_{jk}^+ + b_{jk}^-} (\varphi_y^+ - \varphi_y^-) - \frac{\Delta t}{(a_{jk}^+ + a_{jk}^-)(b_{jk}^+ + b_{jk}^-)} \cdot \\
& \cdot \Big[a_{jk}^- b_{jk}^- H(\widetilde{\varphi}_x(x_{j+}^n, y_{k+}^n, t^n), \widetilde{\varphi}_y(x_{j+}^n, y_{k+}^n, t^n)) + a_{jk}^- b_{jk}^+ H(\widetilde{\varphi}_x(x_{j+}^n, y_{k-}^n, t^n), \widetilde{\varphi}_y(x_{j+}^n, y_{k-}^n, t^n)) \\
& + a_{jk}^+ b_{jk}^- H(\widetilde{\varphi}_x(x_{j-}^n, y_{k+}^n, t^n), \widetilde{\varphi}_y(x_{j-}^n, y_{k+}^n, t^n)) + a_{jk}^+ b_{jk}^+ H(\widetilde{\varphi}_x(x_{j-}^n, y_{k-}^n, t^n), \widetilde{\varphi}_y(x_{j-}^n, y_{k-}^n, t^n)) \Big] \\
& - \frac{a_{jk}^+ a_{jk}^-}{b_{jk}^+ + b_{jk}^-} \left[b_{jk}^+ (\widehat{\varphi}_{xx})_{j,k-}^{n+1} + b_{jk}^- (\widehat{\varphi}_{xx})_{j,k+}^{n+1} \right] \frac{(\Delta t)^2}{2} \\
& - \frac{b_{jk}^+ b_{jk}^-}{a_{jk}^+ + a_{jk}^-} \left[a_{jk}^+ (\widehat{\varphi}_{yy})_{j-,k}^{n+1} + a_{jk}^- (\widehat{\varphi}_{yy})_{j+,k}^{n+1} \right] \frac{(\Delta t)^2}{2} + \mathcal{O}(\Delta t)^2. \qquad (3.10)
\end{aligned}$$

Finally, the limit $\Delta t \to 0$ generates a family of 2D *semi-discrete central-upwind schemes*:

$$\begin{aligned}\frac{\mathrm{d}}{\mathrm{d}t}\varphi_{jk}(t) = &-\frac{a^-_{jk}b^-_{jk}H(\varphi^+_x,\varphi^+_y)+a^-_{jk}b^+_{jk}H(\varphi^+_x,\varphi^-_y)+a^+_{jk}b^-_{jk}H(\varphi^-_x,\varphi^+_y)+a^+_{jk}b^+_{jk}H(\varphi^-_x,\varphi^-_y)}{(a^+_{jk}+a^-_{jk})(b^+_{jk}+b^-_{jk})}\\ &+\frac{a^+_{jk}a^-_{jk}}{a^+_{jk}+a^-_{jk}}\Big(\varphi^+_x-\varphi^-_x\Big)+\frac{b^+_{jk}b^-_{jk}}{b^+_{jk}+b^-_{jk}}\Big(\varphi^+_y-\varphi^-_y\Big)\\ &-\frac{a^+_{jk}a^-_{jk}}{b^+_{jk}+b^-_{jk}}\left[\frac{b^+_{jk}}{2}\lim_{\Delta t\to 0}\Big\{\Delta t(\widehat{\varphi}_{xx})^{n+1}_{j,k-}\Big\}+\frac{b^-_{jk}}{2}\lim_{\Delta t\to 0}\Big\{\Delta t(\widehat{\varphi}_{xx})^{n+1}_{j,k+}\Big\}\right]\\ &-\frac{b^+_{jk}b^-_{jk}}{a^+_{jk}+a^-_{jk}}\left[\frac{a^+_{jk}}{2}\lim_{\Delta t\to 0}\Big\{\Delta t(\widehat{\varphi}_{yy})^{n+1}_{j-,k}\Big\}+\frac{a^-_{jk}}{2}\lim_{\Delta t\to 0}\Big\{\Delta t(\widehat{\varphi}_{yy})^{n+1}_{j+,k}\Big\}\right].\end{aligned}\tag{3.11}$$

We still need to specify $(\widehat{\varphi}_{xx})^{n+1}_{j,k\pm}$ and $(\widehat{\varphi}_{yy})^{n+1}_{j\pm,k}$. If they are proportional to $(\Delta(\varphi_x))^{n+1}/\Delta x$ and to $(\Delta(\varphi_y))^{n+1}/\Delta y$ respectively, then

$$\lim_{\Delta t\to 0}\Big\{\Delta t(\widehat{\varphi}_{xx})^{n+1}_{j,k\pm}\Big\}=0,\quad \lim_{\Delta t\to 0}\Big\{\Delta t(\widehat{\varphi}_{yy})^{n+1}_{j\pm,k}\Big\}=0,$$

and we obtain the original 2D central-upwind scheme from Kurganov *et al.* (2001). However, similarly to the 1D case, we can choose $(\widehat{\varphi}_{xx})^{n+1}_{j,k\pm}$ and $(\widehat{\varphi}_{yy})^{n+1}_{j\pm,k}$ to be proportional to $1/\Delta t$, so that the above limit will not vanish. For example, one can use the minmod limiter:

$$\Delta t(\widehat{\varphi}_{xx})^{n+1}_{j,k\pm}=2\,\mathrm{minmod}\left(\frac{(\widetilde{\varphi}_x)^{n+1}_{j+,k\pm}-\widetilde{\phi}_x(\widehat{x}^n_j,y^n_{k\pm},t^{n+1})}{a^+_{jk}+a^-_{jk}},\frac{\widetilde{\phi}_x(\widehat{x}^n_j,y^n_{k\pm},t^{n+1})-(\widetilde{\varphi}_x)^{n+1}_{j-,k\pm}}{a^+_{jk}+a^-_{jk}}\right),\tag{3.12}$$

$$\Delta t(\widehat{\varphi}_{yy})^{n+1}_{j\pm,k}=2\,\mathrm{minmod}\left(\frac{(\widetilde{\varphi}_y)^{n+1}_{j\pm,k+}-\widetilde{\psi}_y(x_{j\pm},\widehat{y}^n_k,t^{n+1})}{b^+_{jk}+b^-_{jk}},\frac{\widetilde{\psi}_y(x_{j\pm},\widehat{y}^n_k,t^{n+1})-(\widetilde{\varphi}_y)^{n+1}_{j\pm,k-}}{b^+_{jk}+b^-_{jk}}\right),\tag{3.13}$$

where $(\widetilde{\varphi}_x)^{n+1}_{j\pm,k\pm}:=\widetilde{\varphi}_x(x^n_{j\pm},y^n_{k\pm},t^{n+1})$ and $(\widetilde{\varphi}_y)^{n+1}_{j\pm,k\pm}:=\widetilde{\varphi}_y(x^n_{j\pm},y^n_{k\pm},t^{n+1})$. The values of the derivative $\widetilde{\phi}_x$ in (3.12) are given by

$$\widetilde{\phi}_x(\widehat{x}^n_j,y^n_{k\pm},t^{n+1})=\frac{\varphi^{n+1}_{j+,k\pm}-\varphi^{n+1}_{j-,k\pm}}{(a^+_{jk}+a^-_{jk})\Delta t},\tag{3.14}$$

and after using (3.3) and (3.9), we obtain

$$\begin{aligned}\widetilde{\phi}_x(\widehat{x}^n_j,y^n_{k\pm},t^{n+1})=&-\frac{H(\widetilde{\varphi}_x(x^n_{j+},y^n_{k\pm},t^n),\widetilde{\varphi}_y(x^n_{j+},y^n_{k\pm},t^n))-H(\widetilde{\varphi}_x(x^n_{j-},y^n_{k\pm},t^n),\widetilde{\varphi}_y(x^n_{j-},y^n_{k\pm},t^n))}{(a^+_{jk}+a^-_{jk})}\\ &+\frac{a^+_{jk}\varphi^+_x+a^-_{jk}\varphi^-_x}{(a^+_{jk}+a^-_{jk})}+\mathcal{O}(\Delta t).\end{aligned}\tag{3.15}$$

Since the data are smooth along the line segments $(x^n_{j\pm},y^n_{k\pm},t)$, $t^n\leqslant t<t^{n+1}$, it is clear that

$$\lim_{\Delta t\to 0}(\varphi_x)^{n+1}_{j+,k\pm}=\varphi^+_x,\ \lim_{\Delta t\to 0}(\varphi_x)^{n+1}_{j-,k\pm}=\varphi^-_x,\ \lim_{\Delta t\to 0}(\varphi_y)^{n+1}_{j\pm,k+}=\varphi^+_y,\ \lim_{\Delta t\to 0}(\varphi_y)^{n+1}_{j\pm,k-}=\varphi^-_y.\tag{3.16}$$

Therefore using (3.12), (3.16), and (3.15), we obtain

$$\lim_{\Delta t\to 0}\left\{\Delta t(\widehat{\varphi}_{xx})^{n+1}_{j,k\pm}\right\}=\frac{2}{(a^+_{jk}+a^-_{jk})}\,\mathrm{minmod}\left(\varphi^+_x-\varphi^{\mathrm{int}\pm}_x,\varphi^{\mathrm{int}\pm}_x-\varphi^-_x\right),\tag{3.17}$$

where

$$\varphi^{\mathrm{int}\pm}_x:=\frac{a^+_{jk}\varphi^+_x+a^-_{jk}\varphi^-_x}{(a^+_{jk}+a^-_{jk})}-\frac{H(\varphi^+_x,\varphi^\pm_y)-H(\varphi^-_x,\varphi^\pm_y)}{(a^+_{jk}+a^-_{jk})}.\tag{3.18}$$

Likewise, using (3.13), we obtain

$$\lim_{\Delta t\to 0}\left\{\Delta t(\widehat{\varphi}_{yy})^{n+1}_{j\pm,k}\right\}=\frac{2}{(b^+_{jk}+b^-_{jk})}\,\mathrm{minmod}\left(\varphi^+_y-\varphi^{\mathrm{int}\pm}_y,\varphi^{\mathrm{int}\pm}_y-\varphi^-_y\right),\tag{3.19}$$

where

$$\varphi^{\mathrm{int}\pm}_y:=\frac{b^+_{jk}\varphi^+_y+b^-_{jk}\varphi^-_y}{(b^+_{jk}+b^-_{jk})}-\frac{H(\varphi^\pm_x,\varphi^+_y)-H(\varphi^\pm_x,\varphi^-_y)}{(b^+_{jk}+b^-_{jk})}.\tag{3.20}$$

Finally, we substitute (3.17) and (3.19) into (3.11). The resulting 2D *semi-discrete central-upwind scheme* is

$$\begin{aligned}\frac{\mathrm{d}}{\mathrm{d}t}\varphi_{jk}(t)=&-\frac{a^-_{jk}b^-_{jk}H(\varphi^+_x,\varphi^+_y)+a^-_{jk}b^+_{jk}H(\varphi^+_x,\varphi^-_y)+a^+_{jk}b^-_{jk}H(\varphi^-_x,\varphi^+_y)+a^+_{jk}b^+_{jk}H(\varphi^-_x,\varphi^-_y)}{(a^+_{jk}+a^-_{jk})(b^+_{jk}+b^-_{jk})}\\&+a^+_{jk}a^-_{jk}\left[\frac{\varphi^+_x-\varphi^-_x}{a^+_{jk}+a^-_{jk}}-\frac{b^+_{jk}}{b^+_{jk}+b^-_{jk}}\,\mathrm{minmod}\left(\frac{\varphi^+_x-\varphi^{\mathrm{int}-}_x}{a^+_{jk}+a^-_{jk}},\frac{\varphi^{\mathrm{int}-}_x-\varphi^-_x}{a^+_{jk}+a^-_{jk}}\right)\right.\\&\qquad\left.-\frac{b^-_{jk}}{b^+_{jk}+b^-_{jk}}\,\mathrm{minmod}\left(\frac{\varphi^+_x-\varphi^{\mathrm{int}+}_x}{a^+_{jk}+a^-_{jk}},\frac{\varphi^{\mathrm{int}+}_x-\varphi^-_x}{a^+_{jk}+a^-_{jk}}\right)\right]\\&+b^+_{jk}b^-_{jk}\left[\frac{\varphi^+_y-\varphi^-_y}{b^+_{jk}+b^-_{jk}}-\frac{a^+_{jk}}{a^+_{jk}+a^-_{jk}}\,\mathrm{minmod}\left(\frac{\varphi^+_y-\varphi^{\mathrm{int}-}_y}{b^+_{jk}+b^-_{jk}},\frac{\varphi^{\mathrm{int}-}_y-\varphi^-_y}{b^+_{jk}+b^-_{jk}}\right)\right.\\&\qquad\left.-\frac{a^-_{jk}}{a^+_{jk}+a^-_{jk}}\,\mathrm{minmod}\left(\frac{\varphi^+_y-\varphi^{\mathrm{int}+}_y}{b^+_{jk}+b^-_{jk}},\frac{\varphi^{\mathrm{int}+}_y-\varphi^-_y}{b^+_{jk}+b^-_{jk}}\right)\right].\end{aligned}\tag{3.21}$$

Here, $\varphi^{\mathrm{int}\pm}_x$ and $\varphi^{\mathrm{int}\pm}_y$ are given by (3.18) and (3.20), respectively; the one-sided local speeds, $a^\pm_{jk}$ and $b^\pm_{jk}$, are given by (3.2); and formulae for $\varphi^\pm_x$ and $\varphi^\pm_y$ are discussed in Section 3.3 below.

Remark. In practice, for convex Hamiltonians H the one-sided local speeds are computed as

$$\begin{aligned}a^+_{jk}&=\max_\pm\left\{H_x\left(\varphi^\pm_x,\varphi^\pm_y\right),0\right\},\quad a^-_{jk}=\left|\min_\pm\left\{H_x\left(\varphi^\pm_x,\varphi^\pm_y\right),0\right\}\right|,\\b^+_{jk}&=\max_\pm\left\{H_y\left(\varphi^\pm_x,\varphi^\pm_y\right),0\right\},\quad b^-_{jk}=\left|\min_\pm\left\{H_y\left(\varphi^\pm_x,\varphi^\pm_y\right),0\right\}\right|,\end{aligned}\tag{3.22}$$

where the maximum and minimum are taken over all the possible permutations of $\pm$.

3.2 *A three-dimensional scheme*

We consider the three-dimensional (3D) Hamilton–Jacobi equation,

$$\varphi_t + H(\varphi_x, \varphi_y, \varphi_z) = 0.$$

We use the maximal values of the one-sided local speeds of propagation, $a^{\pm}_{jkl}$, $b^{\pm}_{jkl}$, and $c^{\pm}_{jkl}$, in the x-, y- and z-directions, respectively. These values at any grid point (x_j, y_k, z_l) are given by the obvious generalizations of (3.2) and

$$c^{+}_{jkl} := \max_{C_{jkl}} \left\{ H_w(\widetilde{\varphi}_x(x,y,z,t), \widetilde{\varphi}_y(x,y,z,t), \widetilde{\varphi}_z(x,y,z,t)) \right\}_+,$$
$$c^{-}_{jkl} := \left| \min_{C_{jkl}} \left\{ H_w(\widetilde{\varphi}_x(x,y,z,t), \widetilde{\varphi}_y(x,y,z,t), \widetilde{\varphi}_z(x,y,z,t)) \right\}_- \right|,$$

where $C_{jkl} := [x_{j-\frac{1}{2}}, x_{j+\frac{1}{2}}] \times [y_{k-\frac{1}{2}}, y_{k+\frac{1}{2}}] \times [z_{l-\frac{1}{2}}, z_{l+\frac{1}{2}}]$. Proceeding as in two dimensions, the 3D *semi-discrete central-upwind scheme* is (suppressing the indices j, k, l)

$$\begin{aligned}
\frac{\mathrm{d}\varphi}{\mathrm{d}t} &= -\frac{1}{(a^+ + a^-)(b^+ + b^-)(c^+ + c^-)} \sum_{\pm} \left[a^{\pm} b^{\pm} c^{\pm} H(\varphi_x^{\mp}, \varphi_y^{\mp}, \varphi_z^{\mp}) \right] \\
&+ \frac{a^+ a^-}{a^+ + a^-} \left(\varphi_x^+ - \varphi_x^- \right) + \frac{b^+ b^-}{b^+ + b^-} \left(\varphi_y^+ - \varphi_y^- \right) + \frac{c^+ c^-}{c^+ + c^-} \left(\varphi_z^+ - \varphi_z^- \right) \\
&- \frac{1}{(a^+ + a^-)(b^+ + b^-)(c^+ + c^-)} \Bigg\{ a^+ a^- \sum_{\pm} \left[b^{\pm} c^{\pm} (D_x^2 \varphi)^{n+1}_{j,k\mp,l\mp} \right] \\
&+ b^+ b^- \sum_{\pm} \left[a^{\pm} c^{\pm} (D_y^2 \varphi)^{n+1}_{j\mp,k,l\mp} \right] + c^+ c^- \sum_{\pm} \left[a^{\pm} b^{\pm} (D_z^2 \varphi)^{n+1}_{j\mp,k\mp,l} \right] \Bigg\},
\end{aligned} \tag{3.23}$$

where the summations are taken over all possible permutations of $+$ and $-$. For example, in the first sum $a^+ b^- c^+$ should be multiplied by $H(\varphi_x^-, \varphi_y^+, \varphi_z^-)$. In (3.23), we use the notation

$$\begin{aligned}
(D_x^2 \varphi)^{n+1}_{j,k\pm,l\pm} &:= \mathrm{minmod}\left(\varphi_x^+ - (\varphi_x^{\mathrm{int}})_{j,k\pm,l\pm}, (\varphi_x^{\mathrm{int}})_{j,k\pm,l\pm} - \varphi_x^- \right), \\
(D_y^2 \varphi)^{n+1}_{j\pm,k,l\pm} &:= \mathrm{minmod}\left(\varphi_y^+ - (\varphi_y^{\mathrm{int}})_{j\pm,k,l\pm}, (\varphi_y^{\mathrm{int}})_{j\pm,k,l\pm} - \varphi_y^- \right), \\
(D_z^2 \varphi)^{n+1}_{j\pm,k\pm,l} &:= \mathrm{minmod}\left(\varphi_z^+ - (\varphi_z^{\mathrm{int}})_{j\pm,k\pm,l}, (\varphi_z^{\mathrm{int}})_{j\pm,k\pm,l} - \varphi_z^- \right),
\end{aligned}$$

where

$$\begin{aligned}
(\varphi_x^{\mathrm{int}})_{j,k\pm,l\pm} &:= \frac{a^+ \varphi_x^+ + a^- \varphi_x^-}{(a^+ + a^-)} - \frac{H(\varphi_x^+, \varphi_y^{\pm}, \varphi_z^{\pm}) - H(\varphi_x^-, \varphi_y^{\pm}, \varphi_z^{\pm})}{(a^+ + a^-)}, \\
(\varphi_y^{\mathrm{int}})_{j\pm,k,l\pm} &:= \frac{b^+ \varphi_y^+ + b^- \varphi_y^-}{(b^+ + b^-)} - \frac{H(\varphi_x^{\pm}, \varphi_y^+, \varphi_z^{\pm}) - H(\varphi_x^{\pm}, \varphi_y^-, \varphi_z^{\pm})}{(b^+ + b^-)}, \\
(\varphi_z^{\mathrm{int}})_{j\pm,k\pm,l} &:= \frac{c^+ \varphi_z^+ + c^- \varphi_z^-}{(c^+ + c^-)} - \frac{H(\varphi_x^{\pm}, \varphi_y^{\pm}, \varphi_z^+) - H(\varphi_x^{\pm}, \varphi_y^{\pm}, \varphi_z^-)}{(c^+ + c^-)}.
\end{aligned}$$

3.3 *Multidimensional interpolants*

The schemes developed in Sections 3.1 and 3.2 require a multidimensional non-oscillatory reconstruction. The simplest option is to use straightforward multidimensional extensions of the 1D interpolants from Sections 2.2 and 2.3, obtained via a 'dimension-by-dimension' approach.

For example, a 2D non-oscillatory second-order central-upwind scheme is given by (3.21) with

$$\varphi_x^{\pm} = \frac{(\Delta\varphi)^n_{j\pm\frac{1}{2},k}}{\Delta x} \mp \frac{\Delta x}{2}\,(\varphi_{xx})^n_{j+\frac{1}{2},k}, \quad \varphi_y^{\pm} = \frac{(\Delta\varphi)^n_{j,k\pm\frac{1}{2}}}{\Delta y} \mp \frac{\Delta y}{2}\,(\varphi_{yy})^n_{j,k+\frac{1}{2}},$$

$$(\varphi_{xx})^n_{j+\frac{1}{2},k} = \text{minmod}\left(\theta\frac{(\Delta\varphi)^n_{j+\frac{3}{2},k} - (\Delta\varphi)^n_{j+\frac{1}{2},k}}{(\Delta x)^2}, \frac{(\Delta\varphi)^n_{j+\frac{3}{2},k} - (\Delta\varphi)^n_{j-\frac{1}{2},k}}{2(\Delta x)^2}, \theta\frac{(\Delta\varphi)^n_{j+\frac{1}{2},k} - (\Delta\varphi)^n_{j-\frac{1}{2},k}}{(\Delta x)^2}\right),$$

$$(\varphi_{yy})^n_{j,k+\frac{1}{2}} = \text{minmod}\left(\theta\frac{(\Delta\varphi)^n_{j,k+\frac{3}{2}} - (\Delta\varphi)^n_{j,k+\frac{1}{2}}}{(\Delta x)^2}, \frac{(\Delta\varphi)^n_{j,k+\frac{3}{2}} - (\Delta\varphi)^n_{j,k-\frac{1}{2}}}{2(\Delta x)^2}, \theta\frac{(\Delta\varphi)^n_{j,k+\frac{1}{2}} - (\Delta\varphi)^n_{j,k-\frac{1}{2}}}{(\Delta x)^2}\right),$$

where $\theta \in [1, 2]$, and the minmod function is given by (2.12). Similarly, the corresponding 'dimension-by-dimension' 2D extensions of the WENO interpolants from Section 2.3 can be used to reconstruct the derivatives in (3.18), (3.20), and (3.21). For more details see Bryson & Levy (2003d).

4. Numerical examples

In this section, we test the performance of the new semi-discrete central-upwind schemes on a variety of numerical examples. We compare the methods developed in this paper, labelled BKLP, with the second-order scheme from Kurganov *et al.* (2001) and the fifth-order scheme from Bryson & Levy (2003d), both of which are referred to as KNP. Our results demonstrate that the BKLP schemes achieve a better resolution of singularities in comparison with the corresponding KNP schemes.

Note that in regions where the solution is sufficiently smooth, a^+a^- and b^+b^- are either equal to zero or very small (for smooth Hamiltonians and sufficiently small Δx and Δy). Hence, the BKLP and KNP schemes of the same order will be almost identical in these areas, and thus there will be practically no difference in the resolution of smooth solutions. We therefore only examine results after the formation of singularities, for which a^+a^- and/or b^+b^- may be large.

The ODE solver that was used in all our simulations is the fourth-order strong stability preserving Runge–Kutta method (SSP-RK) of Gottlieb *et al.* (2001). Assuming an ODE of the form $\frac{\mathrm{d}}{\mathrm{d}t}\varphi =$

$-H(\nabla\varphi)$ and initial data φ^n, the fourth-order SSP-RK method is

$$\begin{aligned}
\varphi^{(1)} &= \varphi^n - \frac{1}{2}\Delta t H\left(\nabla\varphi^n\right),\\
\varphi^{(2)} &= \frac{649}{1600}\varphi^n + \frac{10890423}{25193600}\Delta t H\left(\nabla\varphi^n\right) + \frac{951}{1600}\varphi^{(1)} - \frac{5000}{7873}\Delta t H\left(\nabla\varphi^{(1)}\right),\\
\varphi^{(3)} &= \frac{53989}{2500000}\varphi^n + \frac{102261}{5000000}\Delta t H\left(\nabla\varphi^n\right) + \frac{4806213}{20000000}\varphi^{(1)}\\
&\quad + \frac{5121}{20000}\Delta t H\left(\nabla\varphi^{(1)}\right) + \frac{23619}{32000}\varphi^{(2)} + \frac{7873}{10000}\Delta t H\left(\nabla\varphi^{(2)}\right),\\
\varphi^{n+1} &= \frac{1}{5}\varphi^n - \frac{1}{10}\Delta t H\left(\nabla\varphi^n\right) + \frac{6127}{30000}\varphi^{(1)} + \frac{1}{6}\Delta t H\left(\nabla\varphi^{(1)}\right) + \frac{7873}{30000}\varphi^{(2)}\\
&\quad + \frac{1}{3}\varphi^{(3)} - \frac{1}{6}\Delta t H\left(\nabla\varphi^{(3)}\right).
\end{aligned} \tag{4.1}$$

The intermediate values of the gradient that are required at every stage of the RK method (4.1) are computed using WENO reconstructions.

4.1 *One-dimensional problems*

A convex Hamiltonian. We first test the performance of our schemes for the Hamilton–Jacobi equation with a convex Hamiltonian:

$$\varphi_t + \frac{1}{2}\left(\varphi_x + 1\right)^2 = 0, \tag{4.2}$$

subject to the periodic initial data $\varphi(x,0) = -\cos(\pi x)$. The change of variables $u(x,t) = \varphi_x(x,t) + 1$ transforms the equation into the Burgers equation $u_t + \frac{1}{2}\left(u^2\right)_x = 0$, which can be easily solved via the method of characteristics. The solution develops a singularity in the form of a discontinuous derivative at time $t = 1/\pi^2$.

The computed solutions at $T = 2{\cdot}5/\pi^2$ (after the singularity formation) are shown in Figure 3, where the second- and fifth-order BKLP and KNP schemes are compared. There is a significant improvement in the resolution of the singularity for the BKLP schemes compared with the KNP schemes. The second-order BKLP scheme has a smaller error at the singularity than the fifth-order KNP scheme, while the fifth-order BKLP scheme has the smallest error. In Table 1 we show the relative L^1- and L^∞-errors.

A non-convex Hamiltonian. In this example, we compute the solution of the 1D Hamilton–Jacobi equation with a non-convex Hamiltonian:

$$\varphi_t - \cos\left(\varphi_x + 1\right) = 0, \tag{4.3}$$

subject to the periodic initial data $\varphi(x,0) = -\cos(\pi x)$. This initial-value problem has a smooth solution for $t \lesssim 1{\cdot}049/\pi^2$, after which a singularity forms. A second singularity forms at $t \approx 1{\cdot}29/\pi^2$. The solutions at time $T = 2/\pi^2$, computed with $N = 100$, are shown in Fig. 4, with a close-up of the singularities in Fig. 5. The convergence results after the singularity formation are given in Table 2. In this example, the local speeds of propagation were estimated by (2.2). The results are similar to the convex case, though the improvement here is somewhat less dramatic.

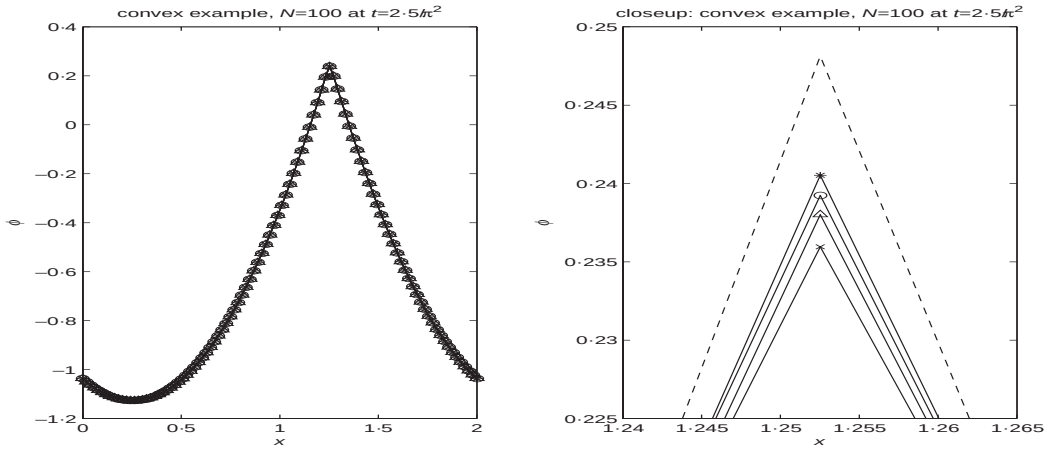

FIG. 3. Problem (4.2). Left: the solution. Right: a close-up of the solution near the singularity. ×: second-order KNP; o: second-order BKLP, △: fifth-order KNP, ∗: fifth-order BKLP. The exact solution is the dashed line.

TABLE 1 *Problem* (4.2). *Relative* L^1*- and* L^∞*-errors for the KNP and BKLP schemes*

Convex example $\varphi_t + \frac{1}{2}(\varphi_x + 1)^2 = 0$				
second-order after singularity $T = 2{\cdot}5/\pi^2$				
	relative L^1-error		relative L^∞-error	
N	KNP	BKLP	KNP	BKLP
100	$3{\cdot}43 \times 10^{-4}$	$2{\cdot}94 \times 10^{-4}$	$1{\cdot}76 \times 10^{-4}$	$1{\cdot}29 \times 10^{-4}$
200	$4{\cdot}57 \times 10^{-5}$	$4{\cdot}10 \times 10^{-5}$	$7{\cdot}00 \times 10^{-6}$	$1{\cdot}96 \times 10^{-6}$
400	$2{\cdot}15 \times 10^{-5}$	$1{\cdot}85 \times 10^{-5}$	$1{\cdot}18 \times 10^{-5}$	$8{\cdot}85 \times 10^{-6}$
800	$2{\cdot}87 \times 10^{-6}$	$2{\cdot}55 \times 10^{-6}$	$4{\cdot}38 \times 10^{-7}$	$1{\cdot}47 \times 10^{-7}$
fifth-order after singularity $T = 2{\cdot}5/\pi^2$				
	relative L^1-error		relative L^∞-error	
N	KNP	BKLP	KNP	BKLP
100	$1{\cdot}50 \times 10^{-4}$	$1{\cdot}13 \times 10^{-4}$	$1{\cdot}46 \times 10^{-4}$	$1{\cdot}10 \times 10^{-4}$
200	$2{\cdot}33 \times 10^{-6}$	$9{\cdot}95 \times 10^{-7}$	$1{\cdot}56 \times 10^{-6}$	$3{\cdot}42 \times 10^{-7}$
400	$9{\cdot}39 \times 10^{-6}$	$7{\cdot}08 \times 10^{-6}$	$9{\cdot}33 \times 10^{-6}$	$7{\cdot}02 \times 10^{-6}$
800	$1{\cdot}13 \times 10^{-7}$	$3{\cdot}94 \times 10^{-8}$	$7{\cdot}54 \times 10^{-8}$	$1{\cdot}41 \times 10^{-8}$

Next, we examine the convergence of the numerical solutions of (4.2) and (4.3), computed by the fifth-order BKLP and KNP schemes. These results, together with the fifth-order methods from Jiang & Peng (2000) and Bryson & Levy (2003c), are shown in Fig. 6. The reader may note that the convergence rates in these examples are erratic. However, this investigation of the relative L^1-errors for many different grid spacings shows that the behaviour is due to super-convergence at some grid spacings. Notice that for all grid spacings the L^1-error of the BKLP method is less than the others.

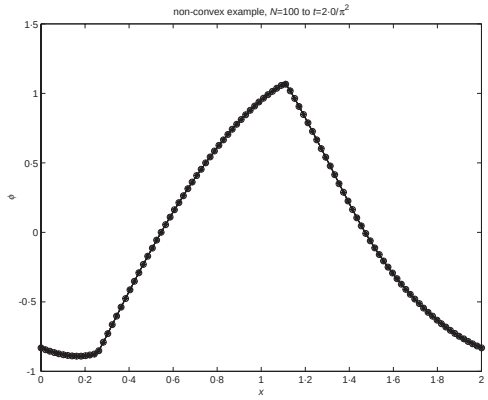

FIG. 4. Problem (4.3): the KNP and BKLP numerical solutions.

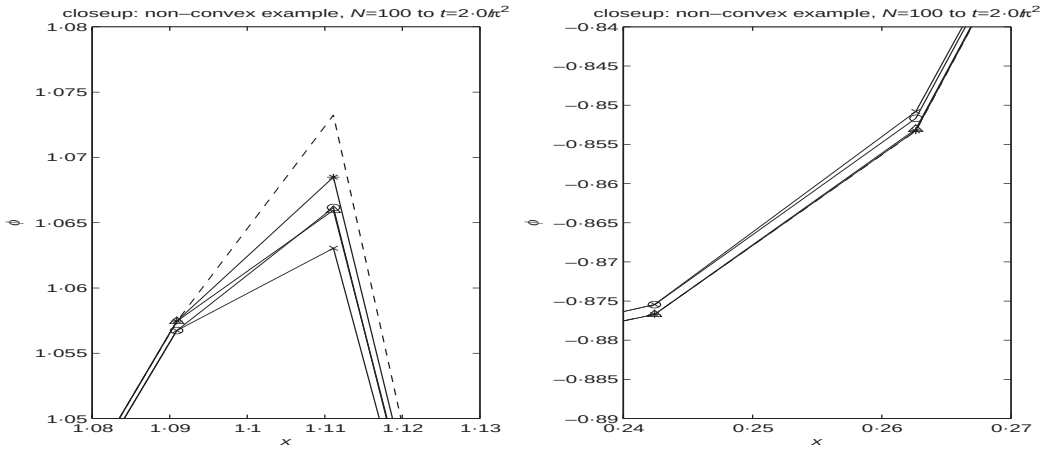

FIG. 5. Problem (4.3). Right: the singularity near $x = 0{\cdot}25$. Left: the singularity near $x = 1{\cdot}11$. $\times$: second-order KNP, o: second-order BKLP, $\triangle$: fifth-order KNP, $*$: fifth-order BKLP. The exact solution is the dashed line.

4.2 *Two-dimensional problems*

In this section, we test the 2D BKLP schemes on Hamilton–Jacobi equations with convex and non-convex Hamiltonians. We start with the convex problem (compare with (4.2))

$$\varphi_t + \frac{1}{2}\left(\varphi_x + \varphi_y + 1\right)^2 = 0, \tag{4.4}$$

which can be reduced to a 1D problem via the coordinate transformation

$$\begin{pmatrix} \xi \\ \eta \end{pmatrix} = \begin{pmatrix} 1/2 & 1/2 \\ 1/2 & -1/2 \end{pmatrix} \begin{pmatrix} x \\ y \end{pmatrix}.$$

The relative L^1- and L^∞-errors for the periodic initial data $\varphi(x, y, 0) = -\cos(\pi(x+y)/2) = -\cos(\pi\xi)$ after the singularity formation at $T = 2{\cdot}5/\pi^2$ are shown in Table 3. The results show that

TABLE 2 *Problem* (4.3). *Relative L^1- and L^∞-errors for the KNP and BKLP schemes*

	Non-convex example $\varphi_t - \cos(\varphi_x + 1) = 0$ second-order after singularity $T = 2{\cdot}0/\pi^2$			
	relative L^1-error		relative L^∞-error	
N	KNP	BKLP	KNP	BKLP
100	$5{\cdot}59 \times 10^{-4}$	$4{\cdot}97 \times 10^{-4}$	$1{\cdot}75 \times 10^{-4}$	$1{\cdot}22 \times 10^{-4}$
200	$9{\cdot}52 \times 10^{-5}$	$9{\cdot}52 \times 10^{-5}$	$4{\cdot}47 \times 10^{-6}$	$4{\cdot}11 \times 10^{-6}$
400	$2{\cdot}40 \times 10^{-5}$	$2{\cdot}40 \times 10^{-5}$	$2{\cdot}06 \times 10^{-6}$	$1{\cdot}57 \times 10^{-6}$
800	$6{\cdot}02 \times 10^{-6}$	$6{\cdot}02 \times 10^{-6}$	$6{\cdot}30 \times 10^{-7}$	$3{\cdot}09 \times 10^{-7}$
	fifth-order after singularity $T = 2{\cdot}0/\pi^2$			
	relative L^1-error		relative L^∞-error	
N	KNP	BKLP	KNP	BKLP
100	$1{\cdot}48 \times 10^{-4}$	$9{\cdot}91 \times 10^{-5}$	$1{\cdot}25 \times 10^{-4}$	$8{\cdot}17 \times 10^{-5}$
200	$8{\cdot}49 \times 10^{-8}$	$5{\cdot}82 \times 10^{-8}$	$1{\cdot}35 \times 10^{-7}$	$8{\cdot}88 \times 10^{-8}$
400	$7{\cdot}89 \times 10^{-9}$	$6{\cdot}60 \times 10^{-9}$	$8{\cdot}21 \times 10^{-7}$	$5{\cdot}48 \times 10^{-7}$
800	$6{\cdot}63 \times 10^{-10}$	$5{\cdot}13 \times 10^{-10}$	$2{\cdot}25 \times 10^{-7}$	$7{\cdot}77 \times 10^{-8}$

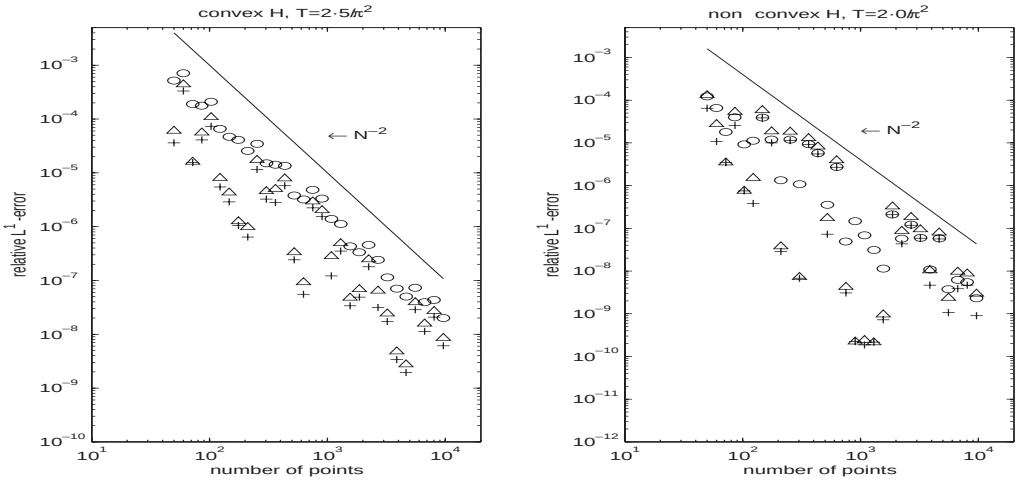

FIG. 6. Convergence of the 1D examples. Left: problem (4.2), $T = 2{\cdot}5/\pi^2$. Right: problem (4.3), $T = 2{\cdot}0/\pi^2$. +: fifth-order BKLP, △: fifth-order KNP, ○: the fifth-order method from Jiang & Peng (2000), The solid lines show example rates of convergence.

while the order of accuracy of the new (reduced dissipation) method does not change, the relative L^1- and L^∞-errors are smaller with the new method (when compared with the results obtained with the method of Kurganov *et al.*, 2001).

In Table 4, we present similar results for the non-convex problem (compare with (4.3))

$$\varphi_t - \cos\left(\varphi_x + \varphi_y + 1\right) = 0, \tag{4.5}$$

with the periodic initial data $\varphi(x, y, 0) = -\cos(\pi(x + y)/2)$. Similarly to the convex case, also with

TABLE 3 *Problem* (4.4). *Relative L^1- and L^∞-errors for the 2D KNP and BKLP schemes*

2D convex example				
second-order after singularity $T = 2{\cdot}5/\pi^2$				
	relative L^1-error		relative L^∞-error	
N	KNP	BKLP	KNP	BKLP
50	$7{\cdot}31 \times 10^{-4}$	$7{\cdot}26 \times 10^{-4}$	$2{\cdot}13 \times 10^{-6}$	$2{\cdot}23 \times 10^{-6}$
100	$3{\cdot}27 \times 10^{-4}$	$2{\cdot}99 \times 10^{-4}$	$1{\cdot}58 \times 10^{-6}$	$1{\cdot}30 \times 10^{-6}$
200	$4{\cdot}37 \times 10^{-5}$	$4{\cdot}12 \times 10^{-5}$	$2{\cdot}34 \times 10^{-8}$	$9{\cdot}87 \times 10^{-9}$
fifth-order after singularity $T = 2{\cdot}5/\pi^2$				
	relative L^1-error		relative L^∞-error	
N	KNP	BKLP	KNP	BKLP
50	$6{\cdot}01 \times 10^{-5}$	$4{\cdot}39 \times 10^{-4}$	$3{\cdot}79 \times 10^{-7}$	$1{\cdot}60 \times 10^{-7}$
100	$1{\cdot}40 \times 10^{-4}$	$1{\cdot}19 \times 10^{-4}$	$1{\cdot}33 \times 10^{-6}$	$1{\cdot}11 \times 10^{-6}$
200	$1{\cdot}98 \times 10^{-6}$	$1{\cdot}23 \times 10^{-6}$	$5{\cdot}97 \times 10^{-9}$	$2{\cdot}58 \times 10^{-9}$

TABLE 4 *Problem* (4.5). *Relative L^1- and L^∞-errors for the 2D KNP and BKLP schemes.*

2D non-convex example				
second-order after singularity $T = 2{\cdot}0/\pi^2$				
	relative L^1-error		relative L^∞-error	
N	KNP	BKLP	KNP	BKLP
50	$1{\cdot}84 \times 10^{-3}$	$1{\cdot}75 \times 10^{-3}$	$5{\cdot}11 \times 10^{-6}$	$3{\cdot}66 \times 10^{-6}$
100	$5{\cdot}86 \times 10^{-4}$	$5{\cdot}48 \times 10^{-4}$	$1{\cdot}50 \times 10^{-6}$	$1{\cdot}21 \times 10^{-6}$
200	$1{\cdot}14 \times 10^{-4}$	$1{\cdot}13 \times 10^{-4}$	$2{\cdot}15 \times 10^{-8}$	$2{\cdot}04 \times 10^{-8}$
fifth-order after singularity $T = 2{\cdot}0/\pi^2$				
	relative L^1-error		relative L^∞-error	
N	KNP	BKLP	KNP	BKLP
50	$1{\cdot}79 \times 10^{-4}$	$1{\cdot}44 \times 10^{-4}$	$6{\cdot}81 \times 10^{-7}$	$6{\cdot}80 \times 10^{-7}$
100	$1{\cdot}14 \times 10^{-4}$	$8{\cdot}97 \times 10^{-5}$	$1{\cdot}02 \times 10^{-6}$	$7{\cdot}82 \times 10^{-7}$
200	$4{\cdot}42 \times 10^{-7}$	$4{\cdot}32 \times 10^{-7}$	$5{\cdot}65 \times 10^{-10}$	$4{\cdot}18 \times 10^{-10}$

the non-convex problem we observe relative L^1- and L^∞-errors that are smaller with the new method than the errors that are obtained with the method of Kurganov *et al.* (2001).

Acknowledgments

The work of AK was supported in part by the NSF Grants DMS-0196439 and DMS-0310585. The work of DL was supported in part by the NSF under Career Grant DMS-0133511. The work of GP was supported in part by the NSF Grant DMS-0296020.

REFERENCES

BARLES, G. & SOUGANIDIS, P. E. (1991) Convergence of approximate schemes for fully nonlinear second order equations. *Asymp. Anal.*, **4**, 271–283.

BRYSON, S. & LEVY, D. (2003a) Central schemes for multidimensional Hamilton–Jacobi equations. *SIAM J. Sci. Comput.*, **25**, 767–791.

BRYSON, S. & LEVY, D. (2003b) High-order central WENO schemes for 1D Hamilton–Jacobi equations. *Numerical Mathematics and Advanced Applications, Proceedings of ENUMATH 2001*. (F. Brezzi *et al.*, eds). Berlin: Springer, pp. 45–54.

BRYSON, S. & LEVY, D. (2003c) High-order central WENO schemes for multi-dimensional Hamilton–Jacobi equations. *SIAM J. Numer. Anal.*, **41**, 1339–1369.

BRYSON, S. & LEVY, D. (2003d) High-order semi-discrete central-upwind schemes for multi-dimensional Hamilton–Jacobi equations. *J. Comput. Phys.*, **189**, 63–87.

CRANDALL, M. G. & LIONS, P.-L. (1984) Two approximations of solutions of Hamilton–Jacobi equations. *Math. Comp.*, **43**, 1–19.

GOTTLIEB, S., SHU, C.-W. & TADMOR, E. (2001) Strong stability-preserving high order time discretization methods. *SIAM Rev.*, **43**, 89–112.

HU, C. & SHU, C.-W. (1999) A discontinuous Galerkin finite element method for Hamilton–Jacobi equations. *SIAM J. Sci. Comput.*, **21**, 666–690.

JIANG, G.-S. & PENG, D. (2000) Weighted ENO schemes for Hamilton–Jacobi equations. *SIAM J. Sci. Comput.*, **21**, 2126–2143.

JIANG, G.-S. & SHU, C.-W. (1996) Efficient implementation of weighted ENO schemes. *J. Comput. Phys.*, **126**, 202–228.

KURGANOV, A. & LIN, C.-T. On the reduction of numerical dissipation in central-upwind schemes. in preparation.

KURGANOV, A. & PETROVA, G. (2000) Central schemes and contact discontinuities. *M2AN Math. Model. Numer. Anal.*, **34**, 1259–1275.

KURGANOV, A. & TADMOR, E. (2000) New high-resolution semi-discrete schemes for Hamilton–Jacobi equations. *J. Comput. Phys.*, **160**, 241–282.

KURGANOV, A., NOELLE, S. & PETROVA, G. (2001) Semidiscrete central-upwind schemes for hyperbolic conservation laws and Hamilton–Jacobi equations. *SIAM J. Sci. Comput.*, **23**, 707–740.

VAN LEER, B. (1979) Towards the ultimate conservative difference scheme, V. A second order sequel to Godunov's method. *J. Comput. Phys.*, **32**, 101–136.

LIN, C.-T. & TADMOR, E. (2000) High-resolution non-oscillatory central schemes for Hamilton–Jacobi Equations. *SIAM J. Sci. Comput.*, **21**, 2163–2186.

LIN, C.-T. & TADMOR, E. (2001) L^1-stability and error estimates for approximate Hamilton–Jacobi solutions. *Numer. Math.*, **87**, 701–735.

LIU, X.-D., OSHER, S. & CHAN, T. (1994) Weighted essentially non-oscillatory schemes. *J. Comput. Phys.*, **115**, 200–212.

OSHER, S. & SETHIAN, J. (1988) Fronts propagating with curvature dependent speed: algorithms based on Hamilton–Jacobi formulations. *J. Comput. Phys.*, **79**, 12–49.

OSHER, S. & SHU, C.-W. (1991) High-order essentially nonoscillatory schemes for Hamilton–Jacobi equations. *SIAM J. Numer. Anal.*, **28**, 907–922.

SOUGANIDIS, P. E. (1985) Approximation schemes for viscosity solutions of Hamilton–Jacobi equations. *J. Differ. Eqns*, **59**, 1–43.

SWEBY, P. K. (1984) High resolution schemes using flux limiters for hyperbolic conservation laws. *SIAM J. Numer. Anal.*, **21**, 995–1011.

Appendix A. Proof of Theorem 2.1

Proof. First, we fix u^- and show that $H^{BKLP}(u,u^-)$ given by (2.22) is a non-increasing function of u (the proof that H^{BKLP} is a non-decreasing function of its second argument is similar). We denote

$$Q(u):=\begin{cases}\dfrac{H(u)-H(u^-)}{u-u^-}, & u\neq u^-,\\[2ex] H'(u^-), & u=u^-,\end{cases} \tag{A.1}$$

and

$$A(u):=\frac{1}{2}\left(a^+(u)-a^-(u)\right),$$

where $a^+(u)=\max\{H'(u),H'(u^-),0\}$ and $a^-(u)=|\min\{H'(u),H'(u^-),0\}|$, and denote by U_1, U_2, V_1, V_2, the sets

$$U_1:=U_1(u^-)=\{u:\ Q(u)-A(u)<0\},\quad U_2:=U_2(u^-)=\{u:\ Q(u)-A(u)\geqslant 0\}, \tag{A.2}$$

$$V_1:=V_1(u^-)=\{u:\ Q(u)-A(u)\leqslant 0\},\quad V_2:=V_2(u^-)=\{u:\ Q(u)-A(u)>0\}. \tag{A.3}$$

Both U_1 and V_2 are open sets (Q and A are continuous) and as such can be represented as a union of at most countably many disjoint open intervals I_j and J_j, respectively, i.e.

$$U_1=\cup_{j=1}^{\infty}I_j\quad\text{and}\quad V_2=\cup_{j=1}^{\infty}J_j. \tag{A.4}$$

In the new notation it is easy to verify that the Hamiltonian H^{BKLP} can be written as

$$H^{BKLP}(u,u^-):=\begin{cases}H_1^{BKLP}(u,u^-), & u\in U_1,\\[2ex] H_2^{BKLP}(u,u^-), & u\in U_2,\end{cases} \tag{A.5}$$

or as

$$H^{BKLP}(u,u^-):=\begin{cases}H_1^{BKLP}(u,u^-), & u\in V_1,\\[2ex] H_2^{BKLP}(u,u^-), & u\in V_2,\end{cases} \tag{A.6}$$

where

$$\begin{aligned}H_1^{BKLP}(u,u^-):=&\frac{a^-(u)H(u^+)+a^+(u)H(u^-)}{a^+(u)+a^-(u)}-\frac{a^+(u)a^-(u)}{a^+(u)+a^-(u)}(u-u^-)\\&+\frac{a^+(u)a^-(u)}{(a^+(u)+a^-(u))^2}(u-u^-)\left[Q(u)+a^-(u)\right],\end{aligned} \tag{A.7}$$

and

$$\begin{aligned}H_2^{BKLP}(u,u^-):=&\frac{a^-(u)H(u^+)+a^+(u)H(u^-)}{a^+(u)+a^-(u)}-\frac{a^+(u)a^-(u)}{a^+(u)+a^-(u)}(u-u^-)\\&+\frac{a^+(u)a^-(u)}{(a^+(u)+a^-(u))^2}(u-u^-)\left[a^+(u)-Q(u)\right].\end{aligned} \tag{A.8}$$

Notice that for those u for which $Q(u) = A(u)$, we have that $H_1^{BKLP}(u, u^-) = H_2^{BKLP}(u, u^-)$, and therefore $H^{BKLP}(\cdot, u^-)$ is a well defined function consisting of the pieces $H_i^{BKLP}(\cdot, u^-)$, $i = 1, 2$. We will use formulae (A.5) and (A.6) and continuity arguments to show that $H^{BKLP}(\cdot, u^-)$ is a non-increasing function on the whole real line.

Consider the point u^* such that $H'(u^*) = 0$ (see assumption (A1)). Then $H_i^{BKLP}(u, u^-)$, $i = 1, 2$, are continuously differentiable on the intervals $(-\infty, \min(u^-, u^*))$, $(\min(u^-, u^*), \max(u^-, u^*))$, and $(\max(u^-, u^*), \infty)$ (in the case $u^- = u^*$, on the first and third interval only) and continuous on $\mathbb{R}$.

CASE 1. Let $u \in (-\infty, \min(u^-, u^*))$. Then $\frac{\mathrm{d}}{\mathrm{d}u}\left(a^+(u)\right) = 0$ since $a^+(u) = \max\{H'(u), H'(u^-), 0\}$ and H' is a non-decreasing function of u. In this case we have

$$\frac{\mathrm{d}}{\mathrm{d}u}\left(H_2^{BKLP}(u, u^-)\right) = -\frac{2(a^-(u))'a^-(u)a^+(u)(u - u^-)}{(a^+(u) + a^-(u))^3}\left[a^+(u) - Q(u)\right] - \frac{(a^-(u))^2(a^+(u) - H'(u))}{(a^+(u) + a^-(u))^2}.$$

Note that there exists $\xi \in (u, u^-)$ such that

$$Q(u) := \frac{H(u) - H(u^-)}{u - u^-} = H'(\xi) \leqslant H'(u^-) \leqslant a^+(u),$$

a^- is a smooth non-increasing function on $(-\infty, \min(u^-, u^*))$, $a^+(u) \geqslant 0$, $a^-(u) \geqslant 0$, $H'(u) \leqslant a^+(u)$, and therefore the derivative $\frac{\mathrm{d}}{\mathrm{d}u}\left(H_2^{BKLP}(u, u^-)\right) \leqslant 0$. Hence $H_2^{BKLP}(u, u^-)$ is non-increasing on $(-\infty, \min(u^-, u^*))$.

Similarly, for $u \in (-\infty, \min(u^-, u^*))$ we have

$$\frac{\mathrm{d}}{\mathrm{d}u}\left(H_1^{BKLP}(u, u^-)\right) = \frac{2(a^-(u))'(a^+(u))^2(u - u^-)}{(a^+(u) + a^-(u))^3}\left[Q(u) - A(u)\right] - \frac{a^-(u)a^+(u)(a^+(u) - H'(u))}{(a^+(u) + a^-(u))^2} + \frac{a^-(u)H'(u)}{a^+(u) + a^-(u)}. \tag{A.9}$$

Now we fix j and consider the corresponding open interval $I_j \cap (-\infty, \min(u^-, u^*))$ (see (A.4) and representation (A.5)). As above, a^- is a smooth non-increasing function on $(-\infty, \min(u^-, u^*))$, $a^+(u) \geqslant 0$, $a^-(u) \geqslant 0$. On each I_j, $Q(u) < A(u)$, and therefore the first term on the right-hand side (RHS) of (A.9) $\leqslant 0$. The second term is non-positive since $a^+(u) \geqslant H'(u)$. The last term is $\leqslant 0$ because $H'(u) \leqslant 0$ for $u \in (-\infty, \min(u^-, u^*))$. This proves that $H_1^{BKLP}(u, u^-)$ is a non-increasing function of u on $I_j \cap (-\infty, \min(u^-, u^*))$, for every j.

CASE 2. Let $u \in (\min(u^-, u^*), \max(u^-, u^*))$. In this case the derivatives are $\frac{\mathrm{d}}{\mathrm{d}u}\left(a^+(u)\right) = 0$ and $\frac{\mathrm{d}}{\mathrm{d}u}\left(a^-(u)\right) = 0$. Therefore

$$\frac{\mathrm{d}}{\mathrm{d}u}\left(H_2^{BKLP}(u, u^-)\right) = -\frac{(a^-(u))^2(a^+(u) - H'(u))}{(a^+(u) + a^-(u))^2} \leqslant 0, \quad \text{since} \quad a^+(u) \geqslant H'(u),$$

which shows that $H_2^{BKLP}(\cdot, u^-)$ is non-increasing on $(\min(u^-, u^*), \max(u^-, u^*))$. Likewise

$$\frac{\mathrm{d}}{\mathrm{d}u}\left(H_1^{BKLP}(u, u^-)\right) = -\frac{a^-(u)a^+(u)(a^+(u) - H'(u))}{(a^+(u) + a^-(u))^2} + \frac{a^-(u)H'(u)}{a^+(u) + a^-(u)}.$$

The first term on the RHS is $\leqslant 0$ since $a^+(u) \geqslant H'(u)$. As for the second term, we have two possibilities. If $u^- < u < u^*$ then $H'(u) < 0$, which will make the whole term $\leqslant 0$. If $u^* < u < u^-$, then $a^-(u) \equiv 0$ and the second term is 0. Therefore, the derivative of H_1^{BKLP} is $\leqslant 0$, and thus $H_1^{BKLP}(\cdot, u^-)$ is non-increasing on $(\min(u^-, u^*), \max(u^-, u^*))$, and in particular on $I_j \cap (\min(u^-, u^*), \max(u^-, u^*))$ for every j.

CASE 3a. Let $u^* \leqslant u^- \leqslant u$. Then $a^-(u) \equiv 0$ and therefore $H^{BKLP} \equiv H_1^{BKLP}(u, u^-) \equiv H_2^{BKLP}(u, u^-) \equiv H(u^-)$. In particular, H_2^{BKLP} is a non-increasing function on (u^-, ∞), and H_1^{BKLP} is a non-increasing function on $I_j \cap (u^-, \infty)$, for every j.

Combining the results from Cases 1, 2 and 3a, we obtain that H_2^{BKLP} is non-increasing on the whole real line (since it is continuous on $\mathbb{R}$ and non-increasing on each of the intervals $(-\infty, \min(u^-, u^*))$, $(\min(u^-, u^*), \max(u^-, u^*))$, and $(\max(u^-, u^*), \infty)$), and H_1^{BKLP} is a non-increasing function on every open interval I_j from U_1 (same reasoning). Since $H_2^{BKLP}(u, u^-) = H_1^{BKLP}(u, u^-)$ for $u \in \partial I_j$ it will follow from (A.5) that $H^{BKLP}(\cdot, u^-)$ is non-increasing on the whole real line.

CASE 3b. Let $u^- \leqslant u^* \leqslant u$. In this case we will utilize representation (A.6) for H^{BKLP} and, using the results from Cases 1 and 2, we will show that H^{BKLP} is a non-increasing function on the interval $[a, b]$ for any a and b, and therefore on the whole real line.

Notice that in this case $V_1 \equiv S^-(u, u^-)$, and then, by assumption (A2), $V_1 \cap [a, b]$ is either empty or a finite number of points and/or a finite union of closed intervals $\mathcal{T}_k$. Note also that we have

$$(u^*, \infty) \cap [a, b] = \cup_{j=1}^{\infty} \left[J_j \cap (u^*, \infty) \cap [a, b] \right] \cup \cup_{k=1}^{m} \mathcal{T}_k, \quad \text{for some} \quad m. \tag{A.10}$$

For $u \in (u^*, \infty)$ we have that $\frac{\mathrm{d}}{\mathrm{d}u}\left(a^-(u)\right) = 0$, and hence

$$\frac{\mathrm{d}}{\mathrm{d}u}\left(H_2^{BKLP}(u, u^-)\right) = -\frac{2(a^+(u))'(a^-(u))^2(u - u^-)}{(a^+(u) + a^-(u))^3}\left[Q(u) - A(u)\right] - \frac{(a^-(u))^2(a^+(u) - H'(u))}{(a^+(u) + a^-(u))^2}.$$

As in Case 1, we fix j and consider this time the corresponding interval $J_j \cap (u^*, \infty)$. Since a^+ is a smooth non-decreasing function on (u^*, ∞) and $Q(u) > A(u)$ on J_j, the first term in the RHS $\leqslant 0$. Also $a^+(u) \geqslant H'(u)$ and hence the second term is also $\leqslant 0$. This gives that $H_2^{BKLP}(u, u^-)$ is a non-increasing function of u on $J_j \cap (u^*, \infty)$ for every j.

When $u^- < u^* < u$, $a^+(u) = H'(u)$, $a^-(u) = -H'(u^-)$, and hence

$$\frac{\mathrm{d}}{\mathrm{d}u}\left(H_1^{BKLP}(u, u^-)\right) = \frac{a^-(u)H'(u)}{(a^+(u) + a^-(u))^3} G(u, u^-), \tag{A.11}$$

where $G(u, u^-)$ is given by (2.20). Since $H'(u) \geqslant 0$ for $u > u^*$, conditions (2.20)–(2.21) ensure that the RHS in (A.11) is $\leqslant 0$ for $u \in \mathcal{T}_k$. This shows that $H_1^{BKLP}(u, u^-)$ is a non-increasing function on each of the intervals $\mathcal{T}_k$ constituting $V_1 \cap [a, b]$ (if $V_1 \cap [a, b]$ consists of a finite number of points, then $H_1^{BKLP} \equiv H_2^{BKLP}$ at these points).

Since $H_1^{BKLP}(u, u^-) = H_2^{BKLP}(u, u^-)$ on ∂J_j, all the above arguments and (A.6) prove that H^{BKLP} is non-increasing on (u^*, ∞). This, together with the conclusion in Cases 1 and 2 and the continuity of $H_i^{BKLP}(u, u^-)$, $i = 1, 2$, gives that H^{BKLP} is non-increasing on $[a, b]$.

Similarly, one proves that $H^{BKLP}(u^+, u)$ (when u^+ is fixed) is a non-decreasing function of the second argument u. Here, in the case corresponding to (A.11) in Case 3b, we have

$$\frac{\mathrm{d}}{\mathrm{d}u}\left(H_2^{BKLP}(u^+, u)\right) = \frac{a^+(u)H'(u)}{(a^+(u) + a^-(u))^3} G(u, u^+), \quad u < u^* < u^+.$$

Since $H'(u) \leqslant 0$ for $u < u^*$, conditions (2.20)–(2.21) guarantee that the derivative is non-negative, and hence $H_2^{BKLP}(u^+, u)$ is a non-decreasing function of u on the finite union of closed intervals $S^+(u, u^+) \cap [a, b]$. □